

# Reconfigurable Intelligent Surfaces with Outdated Channel State Information: Centralized vs. Distributed Deployments

Yan Zhang, Jiayi Zhang, *Senior Member, IEEE*, Marco Di Renzo, *Fellow, IEEE*  
Huahua Xiao, and Bo Ai, *Fellow, IEEE*

## Abstract

In this paper, we investigate the performance of an RIS-aided wireless communication system subject to outdated channel state information that may operate in both the near- and far-field regions. In particular, we take two RIS deployment strategies into consideration: (i) the centralized deployment, where all the reflecting elements are installed on a single RIS and (ii) the distributed deployment, where the same number of reflecting elements are placed on multiple RISs. For both deployment strategies, we derive accurate closed-form approximations for the ergodic capacity, and we introduce tight upper and lower bounds for the ergodic capacity to obtain useful design insights. From this analysis, we unveil that an increase of the transmit power, the Rician- $K$  factor, the accuracy of the channel state information and the number of reflecting elements help improve the system performance. Moreover, we prove that the centralized RIS-aided deployment may achieve a higher ergodic capacity as compared with the distributed RIS-aided deployment when the RIS is located near the base station or near the user. In different setups, on the other hand, we prove that the distributed deployment outperforms the centralized deployment. Finally, the analytical results are verified by using Monte Carlo simulations.

## Index Terms

Reconfigurable intelligent surface (RIS), RIS deployment, near-field, performance analysis.

Y. Zhang and J. Zhang are with the School of Electronic and Information Engineering, Beijing Jiaotong University, Beijing 100044, China.

M. Di Renzo is with Université Paris-Saclay, CNRS, CentraleSupélec, Laboratoire des Signaux et Systèmes, 3 Rue Joliot-Curie, 91192 Gif-sur-Yvette, France.

H. Xiao is with ZTE Corporation, and State Key Laboratory of Mobile Network and Mobile Multimedia Technology, Shenzhen 518057, China.

B. Ai is with the State Key Laboratory of Rail Traffic Control and Safety, Beijing Jiaotong University, Beijing 100044, China.

## I. INTRODUCTION

A reconfigurable intelligent surface (RIS) is an artificial planar structure with integrated electronic circuits, which is equipped with a large number of passive and low-cost scattering elements that can effectively control the wireless propagation environment [1]. By intelligently adapting the phase shifts and the amplitude response of the scattering elements of an RIS, the signals reflected from it can be added constructively or destructively with other signals so as to enhance the signal strength or to suppress the co-channel interference at the receiver [2]–[10]. Thanks to these properties, RISs are considered to be a promising candidate technology for future wireless communication systems.

Several works have investigated the performance of single RIS-aided wireless systems [11]–[35]. In [11], the authors investigated the coverage, the delay outage rate, and the probability of the signal-to-noise-ratio (SNR) gain of an RIS-aided communication system in the presence of Rayleigh fading channels by using the central limit theorem (CLT). A similar system was considered in [12], where the authors studied the coverage probability and the ergodic capacity (EC) by using the moment-matching method. In [13]–[15], the authors proposed accurate closed-form approximations for the outage probability (OP), error rate, and average channel capacity of RIS-aided communication systems over Rayleigh and Rician fading channels, respectively. In [16], the authors derived the asymptotic OP and the achievable rate of an RIS-aided communication system over Rician fading channels. In [17] and [18], the authors provided closed-form approximate expressions for the OP of an RIS-aided communication system. In [19], approximated and upper bound expressions for the bit error rate (BER) were derived over a Nakagami- $m$  fading channel. The authors of [20] and [21] analyzed the BER of an RIS-aided system by taking into account the phase errors caused by the quantization of the phase shifts over Rayleigh and Nakagami fading channels, respectively. In [22] and [23], the authors studied the EC of RIS-assisted communication systems. Particularly, the impact of quantization phase errors was analyzed in [22]. In [24], the minimum required number of phase quantization levels to achieve the full diversity order in RIS-aided communication systems was obtained. In [25], the authors studied the performance of RIS-aided multiple-input multiple-output (MIMO) communication systems with phase noise. A similar system was considered in [26], in which the authors analyzed the OP and throughput of a two-tile RIS-aided wireless network over Rayleigh fading channels. In [27], exact expressions of the OP and the EC for an RIS-aided system over Fox's- $H$  fading

channels were provided. By assuming the same generalized channel model, the authors of [28] analyzed the OP in the presence of phase noise. In [29], the authors studied the asymptotic data rate in an RIS-aided large antenna-array system by considering the channel hardening effects. In [30], the secrecy OP of an RIS-aided communication system was characterized over Rayleigh fading channels. In [31], the end-to-end SNR of an RIS-aided millimeter wave communication system was maximized by optimizing the phase shifts of the RIS elements. In [32], the authors considered an RIS for assisting the communication between two users, and the OP and spectral efficiency were studied over Rayleigh fading channels by using a Gamma approximation. In [33], a closed-form upper bound expression for the EC and an accurate approximation for the OP were derived for transmission over Rician fading channels. In [34], the authors investigated the near- and far-field free-space path loss model for RIS-aided communication systems.

Although previous works have provided important contributions to analyze the performance of RIS-aided systems, most of them can be applied to wireless systems in the presence of a single RIS. More recently, the performance of distributed RIS-aided systems has been investigated in [36]–[41]. In [36], the authors investigated the OP and sum-rate of a dual-hop cooperative network assisted by the RIS which has the highest instantaneous end-to-end SNR among multiple available RISs. In [37], the authors studied multi-RIS-aided systems for application to non-line-of-sight indoor and outdoor communications. In [38], the authors proposed two multi-RIS-aided schemes and provided different approximate methods to analyze the OP and the EC over Nakagami- $m$  fading channels. In [39], the authors studied the OP, the average achievable rate and the average symbol error rate of a distributed RIS-aided communication system. In [40], the authors compared the capacity region of an RIS-aided two-user communication system under centralized and distributed RIS deployment strategies. In [41], the authors proposed an optimization algorithm to configure multiple RISs to maximize the sum-rate of multi-user MIMO communication systems based on statistical channel information (CSI). Although these works have made efforts to investigate distributed RIS-aided communication systems, they have neither analyzed the performance in the near-field region of the RISs, which may not be overlooked in some network deployments [34], nor they have assessed the impact of outdated CSI, which is critical to acquire in RIS-aided systems [42]–[44]. It is worth mentioning that the majority of previous works analyzed the performance of RIS-aided communication systems under the assumption of perfect CSI or statistical CSI to design the optimal phase shifts at the RIS. However, acquiring accurate CSI is very challenging [45]. Due to the associated feedback delay

and the user mobility, the channel learned via estimation may often be outdated. Therefore, it is of great importance to take into account the impact of outdated CSI on the system performance.

Motivated by these considerations, in this paper, we analyze the performance of an RIS-aided communication system by considering two RIS deployment strategies, i.e., the centralized and distributed case, by taking into account the impact of outdated CSI. More specifically, we analyze and compare the system performance over Rician fading channels in both the near- and far-field regions of the RISs. To this end, we derive accurate closed-form approximate expressions for the EC, which can be used in the near- and far-field regions of centralized and distributed RIS deployments, by using the moment-matching method to approximate the cumulative distribution function (CDF) of end-to-end SNR with a Gamma distribution. In order to gain design insights, in addition, we introduce tight lower and upper bounds for the EC. With the aid of the introduced analytical frameworks, we characterize the impact of key parameters on the system performance and compare centralized and distributed RIS deployments against each other. In particular, we show that an increase of the transmit power, the Rician- $K$  factor, the accuracy of CSI and the size of the unit cells results in an improved EC. As a function of the number of RIS elements, we show that the EC increases and reaches a finite limit when the number of RIS elements tends to infinity. This is attributed to the near-field propagation conditions in this asymptotic regime. Furthermore, it is shown that different location deployments for the RISs and CSI accuracy result in different conclusions when comparing the system performance of centralized and distributed deployments. The main contributions of this paper can be summarized as follows.

- We introduce a new analytical framework for the performance analysis of RIS-assisted systems. Considering the impact of outdated CSI, we derive accurate closed-form expressions for the EC in the near- and far-field regions of the RISs. In order to gain additional insights on the impact of the system parameters, we derive tight lower and upper bounds for the EC.
- Capitalizing on the obtained analytical results, we analyze the impact of key system and channel parameters on the performance of RIS-aided systems, from which we conclude that the system performance improves with the transmit power, the Rician- $K$  factor, the CSI accuracy and the size of the reflecting elements. We also observe that the EC does not increase indefinitely when the number of reflecting elements tends to infinity. Furthermore, the relative gains of the centralized and distributed deployments depend on the CSI accuracy and the location of the RISs. The centralized deployment is shown to outperform the

distributed deployment when the RIS is located near the BS or near the user, while the distributed deployment usually offers better performance in the other scenarios.

The remainder of this paper is organized as follows. In Section II, we introduce the system and channel models. In Section III, accurate closed-form approximate expressions for the EC are derived. Moreover, tight upper and lower bounds for the EC are presented. In Section IV, numerical and simulation results are illustrated to confirm the accuracy of the derived expressions. Finally, Section V concludes the paper.

## II. SYSTEM MODEL

As illustrated in Fig. 1, we consider a SISO system in which a fixed single-antenna BS communicates with a single-antenna mobile user with the assistance of  $M$  passive reflecting elements, with each element being capable of independently adjusting its phase shift to reflect the incident signals towards desired directions. Two strategies for deploying the  $M$  reflecting elements are considered: the centralized and distributed deployments. As far as the centralized deployment is concerned, the  $M$  reflecting elements are installed on one RIS. As far as the distributed deployment is concerned, on the other hand, the  $M$  elements are placed on  $L$  ( $L \geq 2$ ) RISs, where the  $l$ -th RIS is equipped with  $M_l$  reflecting elements. It is worth noting that when the BS is sufficiently close to the RIS or the number of reflecting elements of the RIS is very large, the far-field assumption, which means that the channel gain is the same for all the reflecting elements of the RIS, does not hold anymore. In these cases, the RIS operates in the near-field region of the BS. The boundary between the near- and far-field regions of the RIS is conventionally defined as  $D_{\text{boundary}} \triangleq 2D_{\text{RIS}}^2/\lambda$ , where  $D_{\text{boundary}}$  is the distance between the BS and the center of the RIS,  $D_{\text{RIS}}$  is the maximum dimension of the RIS, and  $\lambda$  is the wavelength of the signal. In the next sections, we introduce the near- and far-field system models for the two considered RIS deployment strategies.

### A. Centralized Deployment

In the centralized deployment, we assume that the BS is located in  $(x_t, y_t, z_t)$ , the user is located in  $(x_r, y_r, z_r)$  and the center position of the RIS is  $(x_0, y_0, z_0)$ . The RIS is deployed on a plane that is parallel to the  $xy$ -plane and is equipped with  $M_x \times M_y = M$  reflecting elements. The size of each element along the  $x$  axis and the  $y$  axis is  $d_x$  and  $d_y$ , respectively.

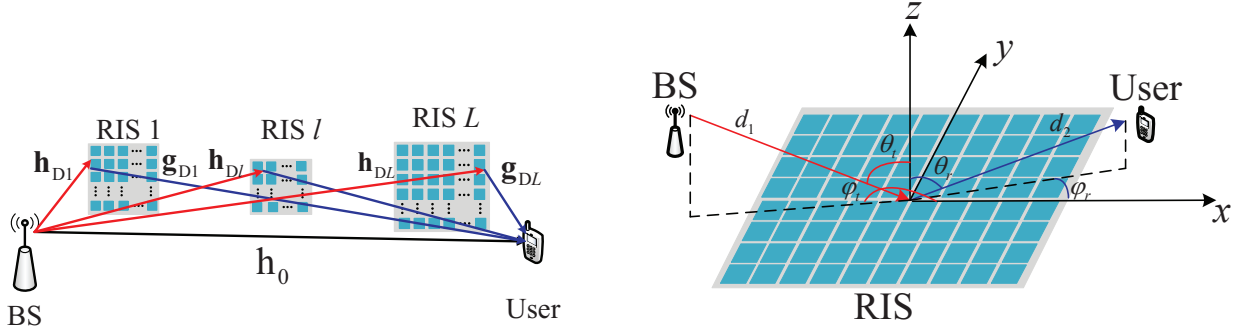


Fig. 1: RIS-aided communication system.

Therefore, the center position of the element of the RIS in the  $y$ -th row and  $x$ -th column is  $(x_0 + (x - \frac{1}{2})d_x, y_0 + (y - \frac{1}{2})d_y, z_0)$ , where  $x \in [1 - M_x/2, M_x/2]$ ,  $y \in [1 - M_y/2, M_y/2]$ .

Due to the user mobility, it is not usually possible to perfectly estimate the CSI at the BS and the RIS (e.g., due to the acquisition delay and the feedback overhead). Therefore, we focus our attention on the impact of outdated CSI on the system performance. We denote by  $h_0$  the direct channel from the BS to the user, by  $\mathbf{h}_C = [h_{C1}, \dots, h_{Cm}, \dots, h_{CM}]^T \in \mathbb{C}^M$  the channel vector from the BS to the RIS, and by  $\mathbf{g}_C = [g_{C1}, \dots, g_{Cm}, \dots, g_{CM}] \in \mathbb{C}^{1 \times M}$  the channel vector from the RIS to the user. More specifically,  $h_0$  and  $\mathbf{g}_C$  can be expressed, respectively, as [43, Eq. (7)], [44, Eq. (12)]

$$h_0 = \rho_0 \hat{h}_0 + \bar{\rho}_0 \omega_0, \quad (1)$$

$$\mathbf{g}_C = \rho_C \hat{\mathbf{g}}_C + \bar{\rho}_C \omega_C. \quad (2)$$

where  $0 \leq \rho_0 \leq 1$  represents the correlation coefficient between the outdated channel estimate  $\hat{h}_0$  and the actual channel  $h_0$ , which can be calculated as  $\rho_0 = J_0(2\pi f_d T_{s0})$  based on Clarke's fading spectrum [43], where  $J_0(\cdot)$  is the zeroth-order Bessel function of the first kind [46, Eq. (8.411)],  $f_d = f_c v/c$  is the maximum Doppler shift,  $f_c$  denotes the carrier frequency,  $v$  denotes the velocity of the user,  $c$  denotes the speed of light, and  $T_{s0}$  is the estimation delay between the actual channel and the outdated channel. In addition,  $\bar{\rho}_0 \triangleq \sqrt{1 - \rho_0^2}$ . Similarly,  $\rho_C = J_0(2\pi f_d T_{sC})$  is the correlation coefficient between the outdated channel  $\hat{\mathbf{g}}_C = [\hat{g}_{C1}, \dots, \hat{g}_{Cm}, \dots, \hat{g}_{CM}] \in \mathbb{C}^{1 \times M}$  and the actual channel  $\mathbf{g}_C$ , and  $\bar{\rho}_C \triangleq \sqrt{1 - \rho_C^2}$ . If  $\rho_i = 1$  ( $i \in \{0, C\}$ ), the CSI is perfect, whereas  $\rho_i = 0$  indicates no CSI. In addition,  $\omega_0 \sim \mathcal{CN}(0, \sigma_{\hat{h}_0}^2)$ , where  $\mathcal{CN}(0, \sigma^2)$  is the complex

Gaussian distribution with zero mean and variance  $\sigma^2$ ,  $\boldsymbol{\omega}_C = [\omega_{C1}, \dots, \omega_{Cm}, \dots, \omega_{CM}] \in \mathbb{C}^{1 \times M}$  with  $\omega_{Cm} \sim \mathcal{CN}(0, \sigma_{\hat{\mathbf{g}}_{Cm}}^2)$  ( $m = 1, \dots, M$ ). We assume that all links experience Rician<sup>1</sup> fading, i.e.,  $\hat{\mathbf{h}}_0 = \sqrt{\frac{K_0}{1+K_0}} \hat{\mathbf{h}}_0^{\text{LoS}} + \sqrt{\frac{1}{1+K_0}} \hat{\mathbf{h}}_0^{\text{NLoS}}$ ,  $\mathbf{h}_C = \sqrt{\frac{K_1}{1+K_1}} \mathbf{h}_C^{\text{LoS}} + \sqrt{\frac{1}{1+K_1}} \mathbf{h}_C^{\text{NLoS}}$  and  $\hat{\mathbf{g}}_C = \sqrt{\frac{K_2}{1+K_2}} \hat{\mathbf{g}}_C^{\text{LoS}} + \sqrt{\frac{1}{1+K_2}} \hat{\mathbf{g}}_C^{\text{NLoS}}$ , where  $K_i$  ( $i \in \{0, 1, 2\}$ ) is the Rician- $K$  factor,  $X^{\text{LoS}}$  ( $X \in \{\hat{\mathbf{h}}_0, \hat{\mathbf{h}}_C, \hat{\mathbf{g}}_C\}$ ) denotes the line-of-sight (LoS) component, and  $X^{\text{NLoS}}$  denotes the non-LoS (NLoS) component. It is worth noting that there exist several efficient channel estimation methods for RIS-assisted communication systems, such as the minimum mean square error [50] and deep learning [51] methods. In this paper, the channel from the BS to the RIS is assumed to be perfectly estimated because the BS and the RIS are assumed to be at fixed locations [42]. As a result, the received signal at the user can be written as

$$\begin{aligned} y_C &= \sqrt{P} \left( \mathbf{g}_C \mathbf{B} \Phi_C \mathbf{h}_C + \sqrt{\beta_0^{-1}} \mathbf{h}_0 \right) s + n_0 \\ &= \sqrt{P} \left( \sum_{m=1}^M \frac{1}{\sqrt{\beta_m}} g_{Cm} h_{Cm} e^{j\varphi_{Cm}} + \frac{1}{\sqrt{\beta_0^{-1}}} h_0 \right) s + n_0, \end{aligned} \quad (3)$$

where  $\mathbf{g}_0 \triangleq \sqrt{\beta_0^{-1}} \mathbf{h}_0$ ,  $P$  is the transmit power,  $n_0$  is the zero-mean additive white Gaussian noise (AWGN) whose variance is  $\sigma_0^2$ ,  $\beta_0$  is the path loss of the direct link,  $\Phi_C = \text{diag}\{e^{j\varphi_{C1}}, \dots, e^{j\varphi_{CM}}\}$  where  $\varphi_{Cm}$  ( $m = 1, \dots, M$ ) is the phase shift of the  $m$ -th element of the RIS, and  $s$  is the transmit signal with unit energy. Moreover,  $\mathbf{B} \triangleq \text{diag}\left\{(\sqrt{\beta_1})^{-1}, \dots, (\sqrt{\beta_M})^{-1}\right\}$  represents the path loss matrix with  $\beta_m$  ( $m = 1, \dots, M$ ) denoting the path loss of the  $m$ -th element of the RIS<sup>2</sup>, which, according to [53], and under the assumption that the peak radiation directions of the transmitting and receiving antennas point towards the center of the RIS, can be expressed as

$$\beta_m \triangleq \beta_0 (r_m^t r_m^r)^2 / F_m^{\text{combine}}, \quad m = 1, 2, \dots, M, \quad (4)$$

where  $\beta_0 \triangleq 16\pi^2 / (G_t G_r d_x^2 d_y^2)$ ,  $G_t$  and  $G_r$  represent the transmit antenna gain and the receive antenna gain, respectively, and  $r_m^t$  and  $r_m^r$  denote the distance between the BS and the  $m$ -th element of the RIS and the distance between the  $m$ -th element of the RIS and the user, respectively. Furthermore,  $F_m^{\text{combine}}$  is the joint normalized power radiation pattern, which depends

<sup>1</sup>It is worth mentioning that the method that we utilize to obtain the derivations of the performance of RIS-assisted systems can be readily applied to other channel fading models (e.g., Nakagami- $m$  [47], [48],  $\kappa - \mu$  [49]). The analysis of different small scale fading models in the near- and far-field regions of RIS-assisted systems is postponed to a future research work.

<sup>2</sup>The generalization of the proposed analytical framework in the presence of channel correlation [52] (i.e.,  $\mathbf{B}$  is a non-diagonal matrix) is left for future research.

on the location of the BS, the RIS, and the user, and is defined as

$$F_m^{\text{combine}} \triangleq (\cos \theta_m^{\text{tx}})^{\frac{G_t}{2}-1} \cos(\theta_m^{\text{t}}) \cos(\theta_m^{\text{r}}) (\cos \theta_m^{\text{rx}})^{\frac{G_r}{2}-1}, \quad (5)$$

where  $\theta_m^{\text{tx}}$  and  $\theta_m^{\text{rx}}$  denote the angles of elevation from the BS antenna and the user antenna to the  $m$ -th reflecting element of the RIS, respectively. In addition,  $\theta_m^{\text{t}}$  and  $\theta_m^{\text{r}}$  represent the angles of elevation from the  $m$ -th reflecting element of the RIS to the BS antenna and user antenna, respectively. According to [53], we have  $\cos \theta_m^{\text{tx}} = \left( d_1^2 + (r_m^{\text{t}})^2 - d_m^2 \right) / (2d_1 r_m^{\text{t}})$ ,  $\cos \theta_m^{\text{rx}} = \left( d_2^2 + (r_m^{\text{r}})^2 - d_m^2 \right) / (2d_2 r_m^{\text{r}})$ ,  $\cos \theta_m^{\text{t}} = (z_t - z_0) / r_m^{\text{t}}$  and  $\cos \theta_m^{\text{r}} = (z_t - z_0) / r_m^{\text{r}}$ , where  $d_1$ ,  $d_2$  and  $d_m$  denote the distance between the BS and the center of the RIS, the distance between the user and the center of the RIS, and the distance between the  $m$ -th element of the RIS and the center of the RIS, respectively. Further details on the path loss model for RIS-aided wireless communications can be found in [53].

By substituting (1) and (2) into (3), we can rewrite the received signal as

$$\begin{aligned} y_C = & \underbrace{\sqrt{P} (\rho_C \hat{\mathbf{g}}_C \mathbf{B} \Phi_C \mathbf{h}_C + \rho_0 \hat{\mathbf{g}}_0)}_{\text{desired signal}} s \\ & + \underbrace{\sqrt{P} \left( \bar{\rho}_C \omega_C \mathbf{B} \Phi_C \mathbf{h}_C + \sqrt{\beta_0^{-1}} \bar{\rho}_0 \omega_0 \right)}_{\text{outdated CSI noise}} s + \underbrace{n_0}_{\text{white noise}}. \end{aligned} \quad (6)$$

effective noise  $n_{\text{Ceff}}$

where  $\hat{\mathbf{g}}_0 \triangleq \sqrt{\beta_0^{-1}} \hat{\mathbf{h}}_0$ . As can be seen from (6), the second term is the outdated CSI noise. Therefore, the effective noise  $n_{\text{Ceff}}$  is composed of the outdated CSI noise and the AWGN, so that the effective transmit SNR can be formulated as  $\gamma_{\text{Cteff}} \triangleq P / \mathbb{E}(|n_{\text{Ceff}}|^2)$ , where  $\mathbb{E}(|n_{\text{Ceff}}|^2)$  is calculated in the next section. Hence, the received SNR at the user can be formulated by using (6) as

$$\gamma_C = \gamma_{\text{Cteff}} |\rho_C \hat{\mathbf{g}}_C \mathbf{B} \Phi_C \mathbf{h}_C + \rho_0 \hat{\mathbf{g}}_0|^2, \quad (7)$$

The phase shifts at the RIS can be designed such that the outdated direct channel (from the BS to the user) and the outdated cascaded channel (from the BS to the RIS and from the RIS to the user) are co-phased, i.e.,  $\varphi_{Cm} = \varphi_{\hat{\mathbf{h}}_0} - (\varphi_{\hat{\mathbf{g}}_{Cm}} + \varphi_{\mathbf{h}_{Cm}})$  for  $m = 1, \dots, M$  [39], and, therefore, the signals via the two channels are constructively added at the user and the received SNR is



maximized. In this case, we obtain

$$\gamma_{\text{Cmax}} = \gamma_{\text{Cteff}} \left( \rho_{\text{C}} \sum_{m=1}^M \sqrt{\beta_m^{-1}} |\hat{\mathbf{g}}_{\text{C}m}| |h_{\text{C}m}| + \rho_0 |\hat{\mathbf{g}}_0| \right)^2. \quad (8)$$

**Far-field case:** The channel in (4) is a general path loss model that can be applied in the near-field and far-field regions of the RIS. In the far-field case, (4) can be simplified since we have  $d_m \ll r_m^{\text{t}} \approx d_1$  and  $d_m \ll r_m^{\text{r}} \approx d_2$ , which results in  $\cos \theta_m^{\text{tx}} \approx 1$  and  $\cos \theta_m^{\text{rx}} \approx 1$ . Therefore, (5) reduces to  $\cos(\theta^{\text{t}}) \cos(\theta^{\text{r}})$  and (4) can be simplified as

$$\beta^{\text{farfield}} \triangleq \beta_0 (d_1 d_2)^2 (\cos(\theta^{\text{t}}) \cos(\theta^{\text{r}})), \quad m = 1, 2, \dots, M, \quad (9)$$

where  $\cos(\theta^{\text{t}}) = (z_{\text{t}} - z_0)/d_1$ ,  $\cos(\theta^{\text{r}}) = (z_{\text{r}} - z_0)/d_2$ . From (9), we see that all the elements of the RIS have the same path loss. When the BS and the user are in the far-field of the RIS, therefore, the received signal can be simplified as

$$\begin{aligned} y_{\text{C}} = & \sqrt{P} \left( \rho_{\text{C}} \left( \sqrt{\beta^{\text{farfield}}} \right)^{-1} \hat{\mathbf{g}}_{\text{C}} \Phi_{\text{C}} \mathbf{h}_{\text{C}} + \rho_0 \hat{\mathbf{g}}_0 \right) \\ & + \underbrace{\sqrt{P} \bar{\rho}_{\text{C}} \left( \sqrt{\beta^{\text{farfield}}} \right)^{-1} \boldsymbol{\omega}_{\text{C}} \Phi_{\text{C}} \mathbf{h}_{\text{C}S}}_{n_{\text{Ceff}}} + \omega_e. \end{aligned} \quad (10)$$

where  $\omega_e \triangleq \sqrt{P} \beta_0^{-1} \bar{\rho}_0 \omega_0 s + n_0$ .

By employing the same phase shift design as that in (8), the optimal received SNR is

$$\gamma_{\text{Cmax}}^{\text{farfield}} = \gamma_{\text{Cteff}}^{\text{farfield}} \left( \rho_{\text{C}} \left( \sqrt{\beta^{\text{farfield}}} \right)^{-1} \sum_{m=1}^M |\hat{\mathbf{g}}_{\text{C}m}| |h_{\text{C}m}| + \rho_0 |\hat{\mathbf{g}}_0| \right)^2, \quad (11)$$

where  $\gamma_{\text{Cteff}}^{\text{farfield}} \triangleq P / \mathbb{E} \left( |n_{\text{Ceff}}^{\text{farfield}}|^2 \right)$ .

### B. Distributed Deployment

In the distributed deployment, we assume that the BS and the user are located in the same positions as those of the centralized deployment. The center position of the  $l$ -th RIS that comprises  $M_{xl} \times M_{yl} = M_l$  reflecting elements is  $(x_{0l}, y_{0l}, z_{0l})$  and all the RISs are deployed parallel to the  $xy$ -plane. Note that all the RISs can be intelligently controlled to reflect the incident signals towards the user so that there is no interference [54] among them [3], [36], [38], [39], [55]. Similar to the centralized deployment, all RIS elements have the same size  $d_x \times d_y$ . Thus, the center position of the element in the  $y$ -th row and  $x$ -th column of the  $l$ -th RIS is

$(x_{0l} + (x - \frac{1}{2})d_x, y_{0l} + (y - \frac{1}{2})d_y, z_{0l})$ , where  $x \in [1 - M_{xl}/2, M_{xl}/2]$ ,  $y \in [1 - M_{yl}/2, M_{yl}/2]$ . Let  $\mathbf{h}_{Dl} = [h_{Dl1}, \dots, h_{Dlm}, \dots, h_{DlM_l}]^T \in \mathbb{C}^{M_l}$  and  $\mathbf{g}_{Dl} = [g_{Dl1}, \dots, g_{Dlm}, \dots, g_{DlM_l}] \in \mathbb{C}^{1 \times M_l}$  denote the channel vectors between the BS and the RIS, and between the RIS and the user, respectively. In the presence of outdated CSI,  $\mathbf{g}_{Dl}$  can be written as

$$\mathbf{g}_{Dl} = \rho_{Dl} \hat{\mathbf{g}}_{Dl} + \bar{\rho}_{Dl} \boldsymbol{\omega}_{Dl}, \quad (12)$$

where  $\hat{\mathbf{g}}_{Dl} = [\hat{g}_{Dl1}, \dots, \hat{g}_{Dlm}, \dots, \hat{g}_{DlM_l}] \in \mathbb{C}^{1 \times M_l}$ ,  $\rho_{Dl}$  is the correlation coefficient between  $\hat{\mathbf{g}}_{Dl}$  and  $\mathbf{g}_{Dl}$ , and  $\bar{\rho}_{Dl} \triangleq \sqrt{1 - \rho_{Dl}^2}$ .  $\boldsymbol{\omega}_{Dl} = [\omega_{Dl1}, \dots, \omega_{Dlm}, \dots, \omega_{DlM_l}] \in \mathbb{C}^{1 \times M_l}$  with  $\omega_{Dlm} \sim \mathcal{CN}(0, \sigma_{\hat{\mathbf{g}}_{Dlm}}^2)$  ( $m = 1, \dots, M_l$ ). In addition, all the links experience Rician fading, from which we have  $\mathbf{h}_{Dl} = \sqrt{\frac{K_{1l}}{1+K_{1l}}} \mathbf{h}_{Dl}^{\text{LoS}} + \sqrt{\frac{1}{1+K_{1l}}} \mathbf{h}_{Dl}^{\text{NLoS}}$  and  $\hat{\mathbf{g}}_{Dl} = \sqrt{\frac{K_{2l}}{1+K_{2l}}} \hat{\mathbf{g}}_{Dl}^{\text{LoS}} + \sqrt{\frac{1}{1+K_{2l}}} \hat{\mathbf{g}}_{Dl}^{\text{NLoS}}$ , where  $K_{1l}$  and  $K_{2l}$  are the Rician- $K$  factors of  $\mathbf{h}_{Dl}$  and  $\hat{\mathbf{g}}_{Dl}$ , respectively,  $Y^{\text{LoS}} \left( Y \in \{\hat{\mathbf{h}}_{Dl}, \hat{\mathbf{g}}_{Dl}\} \right)$  is the LoS component, and  $Y^{\text{NLoS}}$  is the NLoS component. Then, the received signal at the user is

$$y_D = \sqrt{P} \left( \sum_{l=1}^L \mathbf{g}_{Dl} \mathbf{B}_l \Phi_{Dl} \mathbf{h}_{Dl} + \mathbf{g}_0 \right) s + n_0, \quad (13)$$

where  $\Phi_{Dl} = \text{diag}\{e^{j\varphi_{Dl1}}, \dots, e^{j\varphi_{DlM_l}}\}$  denotes the reflection coefficient of the  $l$ -th RIS,  $\mathbf{B}_l \triangleq \text{diag}\{(\sqrt{\beta_{1l}})^{-1}, \dots, (\sqrt{\beta_{lM_l}})^{-1}\}$  is the path loss matrix with  $\beta_{lm}$  ( $m = 1, \dots, M_l, l = 1, \dots, L$ ) denoting the path loss of the  $m$ -th element of the  $l$ -th RIS, which is given by

$$\beta_{lm} \triangleq \beta_0 (r_{lm}^t r_{lm}^r)^2 / F_{lm}^{\text{combine}}, \quad m = 1, 2, \dots, M, l = 1, \dots, L, \quad (14)$$

with

$$F_{lm}^{\text{combine}} \triangleq (\cos \theta_{lm}^{\text{tx}})^{\frac{G_t}{2} - 1} \cos(\theta_{lm}^t) \cos(\theta_{lm}^r) (\cos \theta_{lm}^{\text{rx}})^{\frac{G_r}{2} - 1}, \quad (15)$$

where  $\theta_{lm}^{\text{tx}}$ ,  $\theta_{lm}^{\text{rx}}$ ,  $\theta_{lm}^t$  and  $\theta_{lm}^r$  represent the angle of elevation from the BS antenna to the  $m$ -th reflecting element of the  $l$ -th RIS, the angle of elevation from the user antenna to the  $m$ -th reflecting element of the  $l$ -th RIS, the angle of elevation from the  $m$ -th reflecting element of the  $l$ -th RIS to the BS antenna, and the angle of elevation from the  $m$ -th reflecting element of the  $l$ -th RIS to the user antenna, respectively. From [53], we can write  $\cos \theta_{lm}^{\text{tx}} = (d_{1l}^2 + (r_{lm}^t)^2 - d_{lm}^2) / (2d_{1l}r_{lm}^t)$ ,  $\cos \theta_{lm}^{\text{rx}} = (d_{2l}^2 + (r_{lm}^r)^2 - d_{lm}^2) / (2d_{2l}r_{lm}^r)$ ,  $\cos \theta_{lm}^t = (z_t - z_{0l}) / r_{lm}^t$  and  $\cos \theta_{lm}^r = (z_r - z_{0l}) / r_{lm}^r$ , where  $d_{1l}$ ,  $d_{2l}$ ,  $r_{lm}^t$ ,  $r_{lm}^r$  and  $d_{lm}$  represent the distance between the BS and the  $l$ -th RIS, the distance between the user and the  $l$ -th RIS, the distance between the BS and the  $m$ -th element

of the  $l$ -th RIS, the distance between the user and the  $m$ -th element of the  $l$ -th RIS, and the distance between the  $m$ -th element of the  $l$ -th RIS to the center of the  $l$ -th RIS, respectively. Substituting (12) and (1) into (13), the received signal can be rewritten as

$$y_D = \sqrt{P} \left( \sum_{l=1}^L \rho_{Dl} \hat{\mathbf{g}}_{Dl} \mathbf{B}_{Dl} \Phi_{Dl} \mathbf{h}_{Dl} + \rho_0 \hat{\mathbf{g}}_0 \right) s + \underbrace{\sqrt{P} \sum_{l=1}^L \bar{\rho}_{Dl} \omega_{Dl} \mathbf{B}_{Dl} \Phi_{Dl} \mathbf{h}_{Dl}}_{n_{\text{Dteff}}} s + \omega_e. \quad (16)$$

Therefore, the received SNR can be expressed as

$$\gamma_D = \gamma_{\text{Dteff}} \left| \sum_{l=1}^L \rho_{Dl} \hat{\mathbf{g}}_{Dl} \mathbf{B}_{Dl} \Phi_{Dl} \mathbf{h}_{Dl} + \rho_0 \hat{\mathbf{g}}_0 \right|^2, \quad (17)$$

where  $\gamma_{\text{Dteff}} \triangleq P/\mathbb{E}(|n_{\text{Dteff}}|^2)$  is the effective SNR. The optimal phase-shift matrix that maximizes the received SNR at the user can be expressed as [39]  $\varphi_{lm} = \arg \max_{-\pi \leq \varphi_m \leq \pi} (\theta_{\hat{\mathbf{h}}_0} - (\theta_{\hat{\mathbf{g}}_{Dlm}} + \theta_{\mathbf{h}_{Dlm}}))$ , for  $m = 1, \dots, M_l$  and  $l = 1, \dots, L$ , where  $\theta_{\hat{\mathbf{h}}_0}$ ,  $\theta_{\hat{\mathbf{g}}_{Dlm}}$  and  $\theta_{\mathbf{h}_{Dlm}}$  are the phases of  $\hat{\mathbf{h}}_0$ ,  $\hat{\mathbf{g}}_{Dlm}$  and  $\mathbf{h}_{Dlm}$ , respectively. Hence, the maximum achievable SNR is

$$\gamma_{\text{Dmax}} = \gamma_{\text{Dteff}} \left( \sum_{l=1}^L \sum_{m=1}^{M_l} \rho_{Dl} \sqrt{\beta_{lm}^{-1}} |\hat{\mathbf{g}}_{Dlm}| |\mathbf{h}_{Dlm}| + \rho_0 \hat{\mathbf{g}}_0 \right)^2. \quad (18)$$

**Far-field case:** In the far-field case, similar to the centralized deployment, we obtain  $d_{lm}^2 \leq r_{lm}^t \approx d_{1l}$ ,  $d_{lm}^2 \leq r_{lm}^r \approx d_{2l}$ ,  $\cos \theta_{lm}^{\text{tx}} \approx 1$  and  $\cos \theta_{lm}^{\text{rx}} \approx 1$ , which yields

$$\beta_{Dl}^{\text{farfield}} \triangleq \frac{\beta_0 (d_{1l} d_{2l})^2}{\cos(\theta_l^t) \cos(\theta_l^r)}, l = 1, \dots, L, \quad (19)$$

where  $\cos(\theta_{lm}^t)$  and  $\cos(\theta_{lm}^r)$  can be explicitly expressed as  $\cos(\theta_{lm}^t) = (z_t - z_{0l})/d_{1l}$  and  $\cos(\theta_{lm}^r) = (z_r - z_{0l})/d_{2l}$ , respectively. Equation (19) implies that all the  $M_l$  elements of the  $l$ -th RIS experience the same path loss. Similarly, the received signal in the far-field case can

be formulated as

$$\begin{aligned}
y_D^{\text{farfield}} &= \sqrt{P} \left( \sum_{l=1}^L \rho_{Dl} \left( \sqrt{\beta_{Dl}^{\text{farfield}}} \right)^{-1} \hat{\mathbf{g}}_{Dl} \Phi_{Dl} \mathbf{h}_{Dl} + \rho_0 \hat{\mathbf{g}}_0 \right) s \\
&+ \underbrace{\sum_{l=1}^L \sqrt{P \bar{\rho}_{Dl}} \left( \beta_{Dl}^{\text{farfield}} \right)^{-1} \boldsymbol{\omega}_{Dl} \Phi_{Dl} \mathbf{h}_{Dl}}_{n_{\text{Deff}}^{\text{farfield}}} s + \omega_e.
\end{aligned} \tag{20}$$

By co-phasing the signals from all the distributed RIS elements, similar to (18), the optimal received SNR is

$$\gamma_{\text{Dmax}}^{\text{farfield}} = \gamma_{\text{Dteff}}^{\text{farfield}} \left( \sum_{l=1}^L \rho_{Dl} \left( \sqrt{\beta_{Dl}^{\text{farfield}}} \right)^{-1} \sum_{m=1}^{M_l} |\hat{\mathbf{g}}_{Dlm}| |\mathbf{h}_{Dlm}| + \rho_0 \hat{\mathbf{g}}_0 \right)^2. \tag{21}$$

### III. PERFORMANCE ANALYSIS

The objective of this section is to analyze the performance of the centralized and distributed RIS-aided systems based on  $\gamma_{\text{Cmax}}$ ,  $\gamma_{\text{Cmax}}^{\text{farfield}}$ ,  $\gamma_{\text{Dmax}}$  and  $\gamma_{\text{Dmax}}^{\text{farfield}}$ . However, the computation of the exact distribution of these SNRs is mathematically intractable. To overcome this issue, we introduce approximated expressions of the EC based on the Gamma approximation, whose tightness is substantiated with the aid of numerical results illustrated in Section IV.

#### A. Centralized Deployment

1) *Gamma Approximation:* Let  $\gamma$  be the SNR of interest. The EC normalized by the bandwidth is defined as [22], [23], [33]

$$\bar{C} = \mathbb{E}(\log_2(1+\gamma)) = \int_0^\infty \log_2(1+\gamma) f_\gamma(\gamma) d\gamma \quad \text{bit/s/Hz}. \tag{22}$$

*Corollary 1.* Define  $U_m \triangleq \sqrt{\beta_m^{-1}} |\hat{\mathbf{g}}_{Cm}| |\mathbf{h}_{Cm}|$ ,  $T \triangleq \rho_C \sum_{m=1}^M U_m$ ,  $Z \triangleq T + \rho_0 |\hat{\mathbf{g}}_0|$  and  $R \triangleq Z^2$ . According to [56, Sec. 2.2.2], the probability density function (PDF) of  $Z$  can be tightly approximated by a Gamma distribution as follows

$$f_Z(z) \approx \frac{b_{Z1}^{a_{Z1}}}{\Gamma(a_{Z1})} z^{a_{Z1}-1} e^{-b_{Z1}z}, \tag{23}$$

where  $\Gamma(\cdot)$  is the Gamma function as defined in [46, Eq. (8.310)],  $a_{Z1} \triangleq \frac{(\mathbb{E}(Z))^2}{\text{Var}(Z)}$ ,  $b_{Z1} \triangleq \frac{\mathbb{E}(Z)}{\text{Var}(Z)}$  and  $\text{Var}(Z) = \mathbb{E}(Z^2) - (\mathbb{E}(Z))^2$  with

$$\mathbb{E}(Z) = \rho_C \sum_{m=1}^M \sqrt{\beta_m^{-1}} \Omega_1 \Omega_2 + \sqrt{\beta_0^{-1}} \rho_0 \Omega_0, \quad (24)$$

$$\begin{aligned} \mathbb{E}(Z^2) &= \rho_C^2 \sum_{m=1}^M \beta_m^{-1} + \rho_C^2 \sum_{m=1}^M \sum_{k=1, k \neq m}^M \sqrt{\beta_m^{-1} \beta_k^{-1}} (\Omega_1 \Omega_2)^2 \\ &+ \beta_0^{-1} \rho_0^2 + 2\sqrt{\beta_0^{-1}} \rho_C \rho_0 \sum_{m=1}^M \sqrt{\beta_m^{-1}} \Omega_0 \Omega_1 \Omega_2. \end{aligned} \quad (25)$$

In addition,  $\Omega_0$ ,  $\Omega_1$  and  $\Omega_2$  denote the average values of the Rician variables  $|\hat{h}_0|$ ,  $|h_{Cm}|$  and  $|\hat{g}_{Cm}|$ , respectively, which can be expressed as  $\Omega_i \triangleq \sqrt{\frac{\pi}{4(1+K_i)}} L_{\frac{1}{2}}(-K_i)$  ( $i \in \{0, 1, 2\}$ ) [33, Eq. (12)] with  $L_{\frac{1}{2}}(\cdot)$  being the Laguerre polynomial [57].

*Proof:* See Appendix A. ■

By utilizing  $F_Z(z) = \int_0^\infty f_Z(z) dz$ , we obtain the CDF of  $Z$  as

$$F_Z(z) = 1 - \frac{\Gamma(a_{Z1}, b_{Z1}z)}{\Gamma(a_{Z1})}.$$

where  $\Gamma(\cdot, \cdot)$  is the incomplete gamma function [46, Eq. (8.350.2)]. Since  $\gamma_{C\max} = \gamma_{C\text{teff}} Z^2$ , the CDF of  $\gamma_{C\max}$  can be derived by using the transformation method between two RVs as [58, Eq. (2.1.49)]

$$F_{\gamma_{C\max}}(\gamma) = 1 - \frac{1}{\Gamma(a_{Z1})} \Gamma\left(a_{Z1}, b_{Z1} \sqrt{\frac{\gamma}{\gamma_{C\text{teff}}}}\right). \quad (26)$$

*Corollary 2.* An approximate closed-form expression for the EC of a centralized RIS-aided communication system is given by

$$\bar{C}_{\text{cen}} \approx \frac{2^{a_{Z1}-1}}{\sqrt{\pi} \Gamma(a_1) \ln 2} G_{3,5}^{5,1} \left[ \begin{matrix} b_{Z1}^2 \\ 4\gamma_{C\text{teff}} \end{matrix} \middle| \begin{matrix} \frac{1}{2}, 1, 0 \\ \frac{a_{Z1}}{2}, \frac{a_{Z1}+1}{2}, 0, \frac{1}{2}, 0 \end{matrix} \right], \quad (27)$$

where  $G(\cdot)$  is the Meijer's  $G$ -function [46, Eq. (9.301)]. In addition,  $\gamma_{C\text{teff}} \triangleq \frac{P}{\sigma_{\text{Ceff}}^2}$  with  $\sigma_{\text{Ceff}}^2$

defined as

$$\begin{aligned}\sigma_{\text{Ceff}}^2 &\triangleq \mathbb{E}(|n_{\text{Ceff}}|^2) = P\bar{\rho}_C^2(1 - \Omega_2^2) \sum_{m=1}^M \beta_m^{-1} \\ &\quad + P\bar{\rho}_0^2(1 - \Omega_0^2) \beta_0^{-1} + \sigma_0^2.\end{aligned}\quad (28)$$

*Proof:* See Appendix B. ■

By using (28) and  $\gamma_{\text{Cteff}} \triangleq P/\mathbb{E}(|n_{\text{Ceff}}|^2)$ , we obtain (29), from which we conclude that  $\gamma_{\text{Cteff}}$  tends to be constant when  $P$  tends to infinity.

$$\gamma_{\text{Cteff}} = P \left/ \left( P\bar{\rho}_C^2(1 - \Omega_2^2) \sum_{m=1}^M \beta_m^{-1} + P\bar{\rho}_0^2(1 - \Omega_0^2) \beta_0^{-1} + \sigma_0^2 \right) \right. \quad (29)$$

**Far-field case:** In the far-field regime, from (9), we have  $\beta_m = \beta^{\text{farfield}}$  for  $m = 1, \dots, M$ . With the aid of analytical steps similar to those of Corollary 1 and Corollary 2, the EC can be formulated as

$$\bar{C}_{\text{cen}}^{\text{farfield}} \approx \frac{2^{a_2-1}}{\sqrt{\pi} \Gamma(a_{Z2}) \ln 2} G_{3,5}^{5,1} \left[ \frac{b_{Z2}^2}{4\gamma_{\text{Cteff}}^{\text{farfield}}} \left| \begin{matrix} \frac{1}{2}, 1, 0 \\ \frac{a_{Z2}}{2}, \frac{a_{Z2}+1}{2}, 0, \frac{1}{2}, 0 \end{matrix} \right. \right], \quad (30)$$

where  $a_{Z2} \triangleq \frac{\mathbb{E}((Z^{\text{farfield}})^2)}{\text{Var}(Z^{\text{farfield}})}$ ,  $b_{Z2} \triangleq \frac{\mathbb{E}(Z^{\text{farfield}})}{\text{Var}(Z^{\text{farfield}})}$ ,  $\gamma_{\text{Cteff}}^{\text{farfield}} \triangleq \frac{P}{(\sigma_{\text{Ceff}}^{\text{farfield}})^2}$  and

$$\mathbb{E}(Z^{\text{farfield}}) = \frac{M\rho_C\Omega_1\Omega_2}{\sqrt{\beta^{\text{farfield}}}} + \frac{\rho_0\Omega_0}{\sqrt{\beta_0}}, \quad (31)$$

$$\begin{aligned}\mathbb{E}((Z^{\text{farfield}})^2) &= \frac{M\rho_C^2}{\beta^{\text{farfield}}} + \frac{2M\rho_C\rho_0\Omega_0\Omega_1\Omega_2}{\sqrt{\beta_0}\beta^{\text{farfield}}} \\ &\quad + \frac{M(M-1)\rho_C^2(\Omega_1\Omega_2)^2}{\beta^{\text{farfield}}} + \frac{\rho_0^2}{\beta_0},\end{aligned}\quad (32)$$

$$(\sigma_{\text{Ceff}}^{\text{farfield}})^2 = \frac{PM\bar{\rho}_C^2(1 - \Omega_2^2)}{\beta^{\text{farfield}}} + \frac{P\bar{\rho}_0^2(1 - \Omega_0^2)}{\beta_0} + \sigma_0^2.$$

If  $\rho_C = 1$  and  $h_0 = 0$  (i.e., no outdated CSI and no direct link), the EC reduces to that obtained in [14], as expected.

2) *Bounds for the EC:* Although (27) can be utilized to efficiently evaluate the EC, it is difficult to explicitly analyze the impact of the system and channel parameters on the achievable

performance. Thus, to gain useful design insights, we provide tight upper and lower bounds for the EC by using Jensen's inequality. In particular, the following upper and lower bounds are considered

$$\bar{C}^{\text{lb}} \triangleq \log_2(1 + (\mathbb{E}(1/\gamma))^{-1}) \leq C \leq \bar{C}^{\text{ub}} \triangleq \log_2(1 + \mathbb{E}(\gamma)). \quad (33)$$

*Corollary 3.* The EC of a centralized RIS-aided communication systems is upper bounded by  $\bar{C}^{\text{ub}} = \log_2(1 + \mathbb{E}(\gamma_{\text{Cmax}}))$ , where

$$\begin{aligned} \mathbb{E}(\gamma_{\text{Cmax}}) = & \gamma_{\text{Cteff}} \left( \rho_{\text{C}}^2 \sum_{m=1}^M \beta_m^{-1} + \rho_{\text{C}}^2 \Omega_1^2 \Omega_2^2 \sum_{m=1}^M \sum_{k=1, k \neq m}^M \sqrt{\beta_m^{-1} \beta_k^{-1}} \right. \\ & \left. + 2\rho_{\text{C}} \rho_0 \Omega_0 \Omega_1 \Omega_2 \sqrt{\beta_0^{-1}} \sum_{m=1}^M \sqrt{\beta_m^{-1}} + \rho_0^2 \beta_0^{-1} \right). \end{aligned} \quad (34)$$

Also, the lower bound can be approximated as

$$\bar{C}^{\text{lb}} \approx \log_2 \left\{ 1 + \left( \frac{1}{\mathbb{E}(\gamma_{\text{Cmax}})} + \frac{\text{Var}(\gamma_{\text{Cmax}})}{(\mathbb{E}(\gamma_{\text{Cmax}}))^3} \right)^{-1} \right\}, \quad (35)$$

where

$$\text{Var}(\gamma_{\text{Cmax}}) \approx \frac{\gamma_{\text{Cteff}}^2}{b_{Z_1}^4} \left[ \frac{\Gamma(a_{Z_1} + 4)}{\Gamma(a_{Z_1})} - \frac{\Gamma^2(a_{Z_1} + 2)}{\Gamma^2(a_{Z_1})} \right]. \quad (36)$$

*Proof:* See Appendix C. ■

*Remark 1.* By direct inspection of (32) and (33), we observe that the EC increases when  $\gamma_{\text{Cteff}}$ ,  $\rho_0$  and/or  $\rho_{\text{C}}$  increase. Since  $L_{\frac{1}{2}}(-K_i)$  is a monotonically increasing function of  $K_i$ , in addition,  $\Omega_i$  increases with  $K_i$ , which suggests that the EC is enhanced in the presence of a strong LoS component. If  $K_i \rightarrow \infty$ , i.e., only the LoS components exist in the considered Rician fading channel model, however, the EC of the RIS-assisted system tends to a constant, since, by definition,  $\Omega_i \rightarrow 1$  when  $K_i$  is sufficiently large. If  $K_1 = 0$  or  $K_2 = 0$  and  $K_0 = 0$ , furthermore, we obtain  $\Omega_i = \sqrt{\pi}/2$ . We observe that when the cascaded and direct channels are subject to Rayleigh fading, the EC increases with  $M$ ,  $\rho_0$  and  $\rho_{\text{C}}$ . If  $P \rightarrow \infty$ , also,  $\gamma_{\text{Cteff}}$  tends to a constant. This reveals that the EC does not increase without bound with the transmit power.

**Far-field case:** In the far-field case, we have

$$\begin{aligned} \mathbb{E}(\gamma_{\text{Cmax}}^{\text{farfield}}) &= \gamma_{\text{Cteff}}^{\text{farfield}} \left( M\rho_{\text{C}}^2/\beta^{\text{farfield}} + M(M-1)\rho_{\text{C}}^2\Omega_1^2\Omega_2^2/\beta^{\text{farfield}} \right. \\ &\quad \left. + 2M\rho_{\text{C}}\rho_0\Omega_0\Omega_1\Omega_2/\sqrt{\beta_0\beta^{\text{farfield}}} + \rho_0^2\beta_0^{-1} \right), \end{aligned} \quad (37)$$

$$\text{Var}(\gamma_{\text{Cmax}}^{\text{farfield}}) \approx \frac{(\gamma_{\text{Cteff}}^{\text{farfield}})^2}{b_{Z2}^4} \left[ \frac{\Gamma(a_{Z2}+4)}{\Gamma(a_{Z2})} - \frac{\Gamma^2(a_{Z2}+2)}{\Gamma^2(a_{Z2})} \right]. \quad (38)$$

Substituting (37) into (33) and substituting (38) into (35), we obtain the upper and lower bounds for the EC in the far-field case, respectively. By setting  $K_0 = 0$  and  $\rho_0 = \rho_{\text{C}} = 1$  as a special case, we retrieve the upper bound for the EC in the absence of outdated CSI over a Rayleigh fading channel [33]. Although (37) indicates that the EC increases with the number of elements of the RIS, it needs to be noted that the far-field assumption may no longer hold if  $M$  is very large. In this case, it is necessary to use (34) to accurately estimating the EC.

## B. Distributed Deployment

### 1) Gamma approximation:

*Corollary 4.* Define  $X_{lm} \triangleq \sqrt{\beta_{lm}^{-1}} |\hat{g}_{\text{D}lm}| |h_{\text{D}lm}|$ ,  $Y \triangleq \sum_{l=1}^L \sum_{m=1}^{M_l} \rho_{\text{D}l} X_{lm}$  and  $H \triangleq Y + \rho_0 |\hat{g}_0|$ , then the PDF of  $H$  can be tightly approximated by a Gamma distribution as follows

$$f_H(h) \approx \frac{b_{H1}^{a_{H1}}}{\Gamma(a_{H1})} h^{a_{H1}-1} e^{-b_{H1}h}, \quad (39)$$

where  $a_{H1} \triangleq \frac{(\mathbb{E}(H))^2}{\text{Var}(H)}$ ,  $b_{H1} \triangleq \frac{\mathbb{E}(H)}{\text{Var}(H)}$  and  $\text{Var}(H) = \mathbb{E}(H^2) - (\mathbb{E}(H))^2$  with

$$\mathbb{E}(H) = \sum_{l=1}^L \sum_{m=1}^{M_l} \sqrt{\beta_{lm}^{-1}} \rho_{\text{D}l} \Omega_{1l} \Omega_{2l} + \sqrt{\beta_0^{-1}} \rho_0 \Omega_0. \quad (40)$$

$$\begin{aligned} \mathbb{E}(H^2) &= \sum_{l=1}^L \sum_{m=1}^{M_l} \frac{\rho_{\text{D}l}^2}{\beta_{lm}} + \sum_{l=1}^L \sum_{m=1}^{M_l} \sum_{k=1, k \neq m}^{M_l} \frac{\rho_{\text{D}l}^2 \Omega_{1l}^2 \Omega_{2l}^2}{\sqrt{\beta_{lm} \beta_{lk}}} \\ &\quad + \sum_{l=1}^L \sum_{m=1}^{M_l} \left( \frac{\rho_{\text{D}l} \Omega_{1l} \Omega_{2l}}{\sqrt{\beta_{lm}}} \sum_{j=1, j \neq l}^L \sum_{k=1}^{M_j} \frac{\rho_{\text{D}j} \Omega_{1j} \Omega_{2j}}{\sqrt{\beta_{jk}}} \right) \\ &\quad + \frac{2\rho_0}{\sqrt{\beta_0}} \sum_{l=1}^L \sum_{m=1}^{M_l} \frac{\rho_{\text{D}l} \Omega_{1l} \Omega_{2l}}{\sqrt{\beta_{lm}}} + \frac{\rho_0^2}{\beta_0}, \end{aligned} \quad (41)$$



where  $\Omega_{1l}$  and  $\Omega_{2l}$  denote the average values of the Rician variables  $|h_{Dlm}|$  and  $|\hat{g}_{Dlm}|$ , respectively, which can be expressed as  $\Omega_{il} \triangleq \sqrt{\frac{\pi}{4(1+K_{il})}} L_{\frac{1}{2}}(-K_{il})$  ( $i \in \{1, 2\}$ ).

*Proof:* See Appendix D. ■

By exploiting a similar methodology as for the derivation of (26), we arrive at

$$F_{\gamma_{D\max}}(\gamma) = 1 - \frac{1}{\Gamma(a_{H1})} \Gamma\left(a_{H1}, b_{H1} \sqrt{\frac{\gamma}{\gamma_{D\text{teff}}}}\right). \quad (42)$$

*Corollary 5.* An approximated closed-form expression for the EC of a distributed RIS-aided communication system is given by

$$\bar{C}_{\text{dis}} \approx \frac{2^{a_{H1}-1}}{\sqrt{\pi} \Gamma(a_{H1}) \ln 2} G_{3,5}^{5,1} \left[ \frac{b_{H1}^2}{4\gamma_{D\text{teff}}} \left| \begin{array}{c} \frac{1}{2}, 1, 0 \\ \frac{a_{H1}}{2}, \frac{a_{H1}+1}{2}, 0, \frac{1}{2}, 0 \end{array} \right. \right], \quad (43)$$

where  $\gamma_{D\text{teff}} \triangleq P/\sigma_{\text{Deff}}^2$  and

$$\sigma_{\text{Deff}}^2 \triangleq P \sum_{l=1}^L \sum_{m=1}^{M_l} \frac{\bar{\rho}_{Dl}^2 (1 - \Omega_{2l}^2)}{\beta_{lm}} + \frac{P \bar{\rho}_0^2 (1 - \Omega_0^2)}{\beta_0} + \sigma_0^2. \quad (44)$$

*Proof:* See Appendix E. ■

By setting  $L = 1$ , (43) reduces to the EC of the centralized RIS deployment in (27)

**Far-field case:** By setting  $\beta_{lm} = \beta_{Dl}^{\text{farfield}}$ , we can obtain the EC for the distributed deployment in the far-field regime

$$\bar{C}_{\text{dis}}^{\text{farfield}} = \frac{2^{a_{H2}-1}}{\sqrt{\pi} \Gamma(a_{H2}) \ln 2} G_{3,5}^{5,1} \left[ \frac{b_{H2}^2}{4\gamma_{D\text{teff}}^{\text{farfield}}} \left| \begin{array}{c} \frac{1}{2}, 1, 0 \\ \frac{a_{H2}}{2}, \frac{a_{H2}+1}{2}, 0, \frac{1}{2}, 0 \end{array} \right. \right], \quad (45)$$

where  $a_{H2} \triangleq \frac{(\mathbb{E}(H^{\text{farfield}}))^2}{\text{Var}(H^{\text{farfield}})}$  and  $b_{H2} \triangleq \frac{E(H^{\text{farfield}})}{\text{Var}(H^{\text{farfield}})}$ . Moreover, we have

$$\mathbb{E}(H^{\text{farfield}}) = \sum_{l=1}^L \sum_{m=1}^{M_l} \frac{\rho_{Dl} \Omega_{1l} \Omega_{2l}}{\sqrt{\beta_{Dl}^{\text{farfield}}}} + \frac{\rho_0 \Omega_0}{\sqrt{\beta_0}}, \quad (46)$$

$$\begin{aligned} \mathbb{E}\left((H^{\text{farfield}})^2\right) &= \frac{\rho_0^2}{\beta_0} + \sum_{l=1}^L \frac{M_l \rho_{Dl}^2}{\sqrt{\beta_{Dl}^{\text{farfield}}}} + \sum_{l=1}^L \frac{M_l (M_l - 1) \rho_{Dl}^2 \Omega_{1l}^2 \Omega_{2l}^2}{\beta_{Dl}^{\text{farfield}}} \\ &+ 2 \sum_{l=1}^L \frac{M_l \rho_{Dl} \rho_0 \Omega_0 \Omega_{1l} \Omega_{2l}}{\sqrt{\beta_0 \beta_{Dl}^{\text{farfield}}}} + \sum_{l=1}^L \left( \frac{M_l \rho_{Dl} \Omega_{1l} \Omega_{2l}}{\sqrt{\beta_{Dl}^{\text{farfield}}}} \sum_{j=1, j \neq l}^L \frac{M_j \rho_{Dj} \Omega_{1j} \Omega_{2j}}{\sqrt{\beta_{Dj}^{\text{farfield}}}} \right). \end{aligned}$$

2) *Bounds for the EC:*

*Corollary 6.* The EC of a decentralized RIS-aided communication systems is upper bounded by

$$\begin{aligned} \mathbb{E}(\gamma_{\text{Dmax}}) = & \gamma_{\text{Deff}} \left( \frac{\rho_0^2}{\beta_0} + \sum_{l=1}^L \sum_{m=1}^{M_l} \frac{\rho_{\text{D}l}^2}{\beta_{lm}} + 2 \sum_{l=1}^L \sum_{m=1}^{M_l} \frac{\rho_{\text{D}l} \rho_0 \Omega_0 \Omega_{1l} \Omega_{2l}}{\sqrt{\beta_0 \beta_{lm}}} \right. \\ & + \sum_{l=1}^L \sum_{m=1}^{M_l} \sum_{k=1, k \neq m}^{M_l} \frac{\rho_{\text{D}l}^2 \Omega_{1l}^2 \Omega_{2l}^2}{\sqrt{\beta_{lm} \beta_{lk}}} \\ & \left. + \sum_{l=1}^L \sum_{m=1}^{M_l} \left( \frac{\rho_{\text{D}l} \Omega_{1l} \Omega_{2l}}{\sqrt{\beta_{lm}}} \sum_{j=1, j \neq l}^L \sum_{k=1}^{M_j} \frac{\rho_{\text{D}j} \Omega_{1j} \Omega_{2j}}{\sqrt{\beta_{jk}}} \right) \right). \end{aligned} \quad (47)$$

Also, the lower bound can be approximated as

$$\text{Var}(\gamma_{\text{Dmax}}) = \frac{\gamma_{\text{Dteff}}^2}{b_{H1}^4} \left[ \frac{\Gamma(a_{H1} + 4)}{\Gamma(a_{H1})} - \frac{\Gamma^2(a_{H1} + 2)}{\Gamma^2(a_{H1})} \right]. \quad (48)$$

*Proof:* See Appendix F. ■

**Far-field case:** In the far-field case, the EC can be approximated as follows

$$\begin{aligned} \mathbb{E}(\gamma_{\text{Dmax}}^{\text{farfield}}) = & \gamma_{\text{Deff}}^{\text{farfield}} \left( \frac{\rho_0^2}{\beta_0} + \sum_{l=1}^L \frac{M_l \rho_{\text{D}l}^2}{\beta_{\text{D}l}^{\text{farfield}}} + 2 \sum_{l=1}^L \frac{M_l \rho_{\text{D}l} \rho_0 \Omega_0 \Omega_{1l} \Omega_{2l}}{\sqrt{\beta_0 \beta_{\text{D}l}^{\text{farfield}}}} \right. \\ & + \sum_{l=1}^L \frac{M_l (M_l - 1) \rho_{\text{D}l}^2 \Omega_{1l}^2 \Omega_{2l}^2}{\beta_{\text{D}l}^{\text{farfield}}} \\ & \left. + \sum_{l=1}^L \left( \frac{M_l \rho_{\text{D}l} \Omega_{1l} \Omega_{2l}}{\sqrt{\beta_{\text{D}l}^{\text{farfield}}}} \sum_{j=1, j \neq l}^L \frac{M_j \rho_{\text{D}j} \Omega_{1j} \Omega_{2j}}{\sqrt{\beta_{\text{D}j}^{\text{farfield}}}} \right) \right), \end{aligned} \quad (49)$$

$$\text{Var}(\gamma_{\text{Dmax}}^{\text{farfield}}) \approx \frac{(\gamma_{\text{Dteff}}^{\text{farfield}})^2}{b_{H2}^4} \left[ \frac{\Gamma(a_{H2} + 4)}{\Gamma(a_{H2})} - \frac{\Gamma^2(a_{H2} + 2)}{\Gamma^2(a_{H2})} \right]. \quad (50)$$

From (49), we can infer similar performance trends as for the centralized deployment.

#### IV. NUMERICAL RESULTS

In this section, we compare the analytical results against Monte Carlo simulations. The simulation parameters are provided in Table I. In addition, the path loss of the direct link is modeled as  $\beta_0^{-1} [\text{dB}] = \eta - 10\xi \log_{10}(d_0)$ , where  $\eta = -30\text{dB}$  is a reference path loss,  $\xi = 3.5$  is the path loss exponent, and  $d_0$  is the distance from the BS to the user.

In Fig. 2, the accuracy of the Gamma approximation as well as the tightness of the upper and lower bounds for the EC are examined. In the centralized deployment, the RIS is located

TABLE I: Simulation parameters

Parameter	Value
Location of the BS $(x_t, y_t, z_t)$	$(-50, 0, 10)$ m
Location of the user $(x_r, y_r, z_r)$	$(50, 0, 10)$ m
Carrier frequency	$f_c = 5$ GHz
Noise power	$\sigma_0^2 = -120$ dBm
Size of RIS elements	$d_x = d_y \in [\lambda/10, \lambda/2]$
Antenna gains at the BS and user	$G_t = 20$ dB, $G_r = 0$ dB

in  $(-49.5, 0, 9.5)$ . The size of all the RIS elements is  $\lambda/8 \times \lambda/8$ . It can be observed from Fig. 2 that the Gamma approximation provides an almost perfect match with the simulated results. Furthermore, it can be seen that the performance gap between the upper and lower bounds and Monte Carlo simulations diminishes as the number of reflecting elements  $M$  increases, which confirms the accuracy of the bounds. Moreover, we observe that the EC increases as the Rician- $K$  factor of the direct link increases. In addition, the gap between the Monte Carlo results and the upper and lower bounds decreases with the increase of the Rician  $K$ -factor. Also, it can be seen that the EC first improves with an increase of the transmit power  $P$ . When  $P$  is sufficiently large, however, the capacity tends to a limit, which can be explained by the fact that the equivalent SNR tends to be constant as  $P$  increases. The results validate the correctness of *Remark 1*.

In Fig. 3, we analyze the EC as a function of the correlation coefficient  $\rho$  and the size  $d_x \times d_y$  of the reflecting elements of RIS. For the centralized deployment, the RIS is located in  $(-49.5, 0, 9.5)$  with  $M = M_x \times M_y = 24 \times 24 = 576$  elements. For the distributed deployment, on the other hand, we consider two RISs located in  $(-49, 0, 9.5)$  and  $(49, 0, 9.5)$ , respectively. In addition, the two RISs are equipped with  $M_{xi} \times M_{yi} = 16 \times 18 = 288$  ( $i \in \{1, 2\}$ ) elements, thus the total number of RIS elements is the same as for the centralized deployment. We assume  $\rho_1 = \rho_2 = \rho$ . It can be observed from Fig. 3 that the accuracy of the bounds and the Gamma approximation is demonstrated. Furthermore, the EC decreases as  $\rho$  decreases (i.e., the CSI becomes more outdated) for both the centralized and distributed deployments. Moreover, we find that increasing the size of the reflecting elements can significantly improve the system performance.

In Fig. 4, we present the EC in the near- and far-field regions for the centralized RIS deployment by using the general expression in (27) and the far-field expression in (30). The boundary between the near-field and the far-field region is calculated as  $D_{\text{boundary}} = 2 \left( (M_x d_x)^2 + (M_y d_y)^2 \right) / \lambda$ .

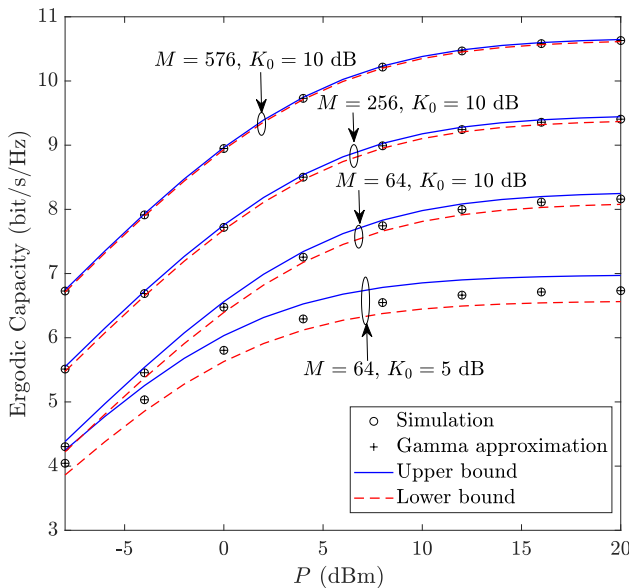


Fig. 2: EC versus  $P$  for different values of  $K_0$  for centralized and distributed RIS deployments ( $\rho_0 = 0.95$ ,  $\rho_C = 0.9$ ,  $\rho_{D1} = \rho_{D2} = 0.9$ ).

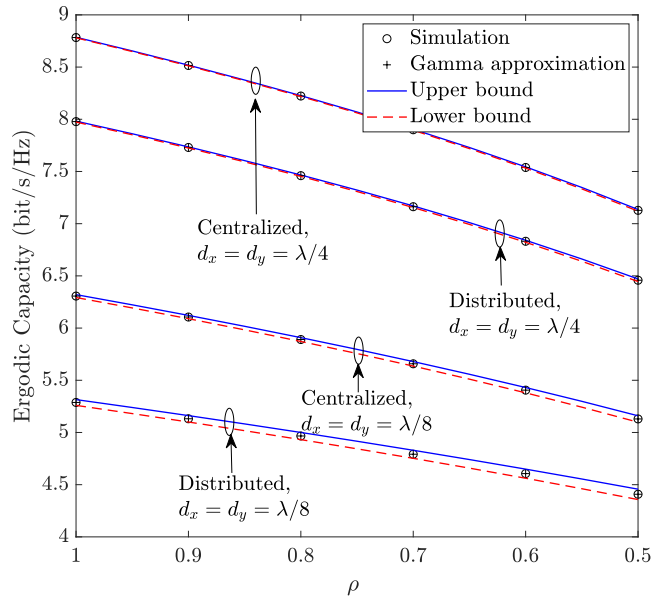


Fig. 3: EC versus  $\rho$  for different sizes of reflecting elements of RIS for centralized and distributed RIS deployments ( $\rho_0 = 0.95$ ).

For example,  $D_{\text{boundary}}$  can be calculated as 6 m, 4.7 m, and 3.75 m for  $M_x = M_y = 40$ ,  $M_x = 30, M_y = 40$ , and  $M_x = 20, M_y = 40$  if  $d_x = d_y = \lambda/8$ , respectively. As observed from the figure, in the near-field region, there is a performance gap between the two formulas, and the gap increases with the increase of the total number of RIS elements. This indicates that it is inaccurate to use the far-field formula to analyze the EC if the BS or the user is in the near-field of the RIS. Furthermore, we observe that the far-field formula gradually approaches the general formula as the distance between the BS and the RIS increases: when  $d_1 > D_{\text{boundary}}$ , the two curves almost coincide.

Figure 5 illustrates the impact of the size of the unit cells ( $d_x \times d_y$ ) on the system performance. We assume that the BS is in the near-field of the RIS, and the RIS has  $24 \times 24$  reflecting elements. We can observe from this figure that the larger the size of the unit cells of the RIS, the better the system performance. This is due to the fact that the total size of the RIS increases when the size of the unit increases while keeping fixed the number of unit cells.

Figure 6 shows the EC in the near- and far-field regimes for the centralized RIS deployment as a function of the total number of RIS reflecting elements. We set  $M_x = 24$  fixed and increase  $M_y$  linearly. In the near-field regime, the RIS is located in  $(-49.5, 0, 9.5)$ , and in the far-field

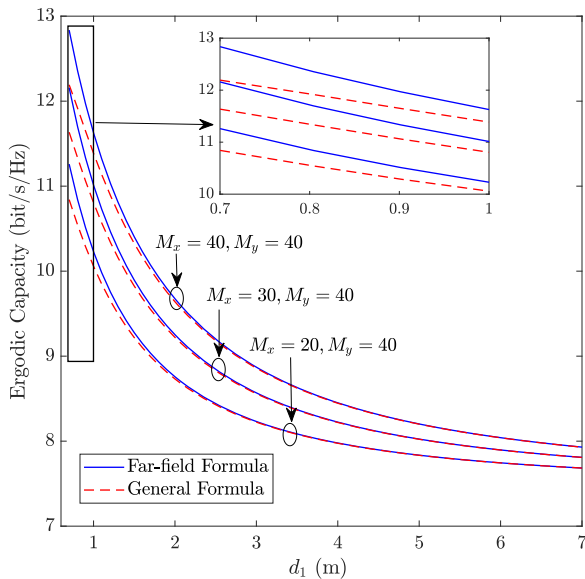


Fig. 4: Comparison of the EC performance in the near- and far-field cases for the centralized deployment ( $d_x = d_y = \frac{\lambda}{8}$ ,  $\rho_0 = 0.95$ ,  $\rho_C = 0.9$ ).

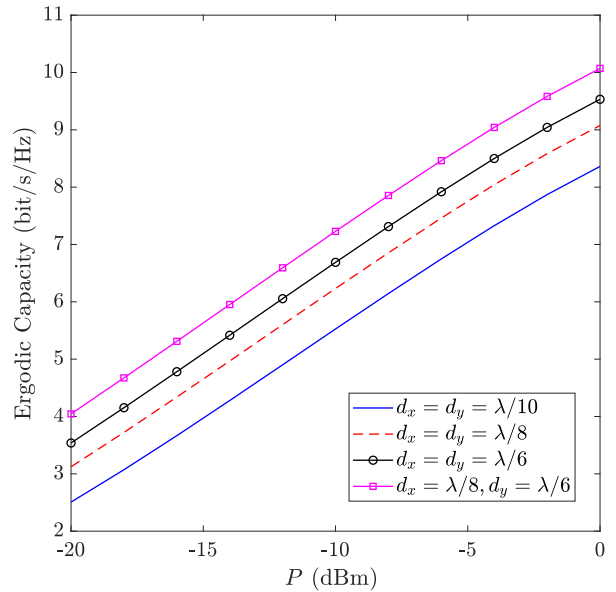


Fig. 5: EC versus  $P$  for a different size of the unit cells for the centralized RIS deployment in the near-field case ( $\rho_0 = 0.95$ ,  $\rho_C = 0.9$ ,  $M_x = M_y = 24$ ).

regime, the location of the RIS is  $(0, 0, 9.5)$ . We observe that when the BS is in the far-field of the RIS, the EC increases with an increase of the number of RIS reflecting elements. When the BS is in the near-field of the RIS, on the other hand, the EC first increases with the number of RIS reflecting elements and then tends towards a constant limit. This performance trend can be explained as follows: If the BS and the receiver are steered towards the center of the RIS, the RIS reflecting elements that are closer to the edge of the RIS experience a more severe path loss compared to those that are closer to the center of the RIS. Therefore, their contribution to the EC is not significant [34], [53].

In Fig. 7, we analyze how different shapes of the RIS affect the EC with a fixed total number of reflecting elements of the RIS. As can be readily observed, the more concentrated the reflecting elements installed on the RIS, i.e., the closer the shape of the RIS to a square is, the better the system performance in the near-field regime. For example, if  $P = -10$  dBm, setting  $M_x = M_y = 24$  results in 1.87% and 4.78% of improvement of the EC compared to  $M_x = 16, M_y = 36$  and  $M_x = 12, M_y = 48$ , respectively. In addition, we observe that the shape of the RIS has no impact on the EC in the far-field regime, because all the elements experience approximately the

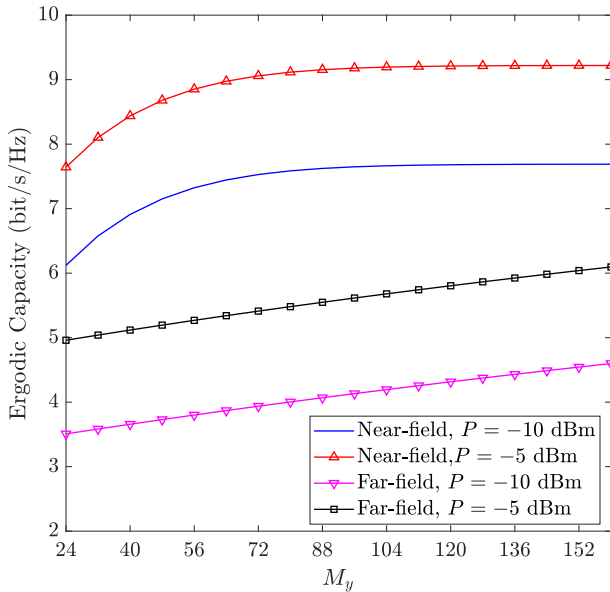


Fig. 6: EC versus  $M_y$  for different values of the transmit power in the near- and far-field regions for the centralized RIS deployment ( $M_x = 24$ ,  $\rho_0 = 0.95$ ,  $\rho_C = 0.9$ ).

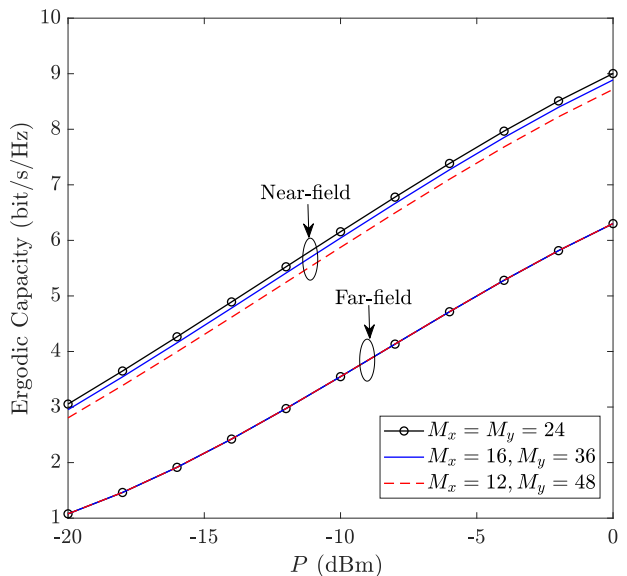


Fig. 7: Comparison of the EC performance for different shapes of the RIS in the near- and far-field regimes ( $\rho_0 = 0.95$ ,  $\rho_C = 0.9$ ).

same path loss in the far-field regime, while in the near-field case the path loss of each element is different.

In Fig. 8, we analyze the impact on the EC of the centralized and distributed deployments. As for the centralized deployment, the single RIS is moved along the  $x$ -axis from the BS to the user. As for the distributed deployment, we consider the following three different cases, as illustrated in Fig. 8 (a). In case 1 and case 2, the two RISs are located near the BS and the user, respectively, and the distance between the two RISs is 0.5 m. In case 3, on the other hand, one RIS is located near the BS and the other RIS is located near the user. We observe from Fig. 8 (b) and Fig. 8 (c) that the EC degrades as  $\rho$  decreases, since a smaller value of  $\rho$  implies a less accurate CSI. Furthermore, in all distributed deployment cases, the EC is the largest in case 3. On the other hand, the scenario where the RIS is located near the user yields a better EC than the case where the RIS is located near the BS. In addition, it is found that the distributed deployment outperforms the centralized deployment. The two deployments provide almost the same performance when a single RIS is located either near the BS or the user. Moreover, the EC decreases as  $K_0$  decreasing, and the conclusions of the comparison between the centralized

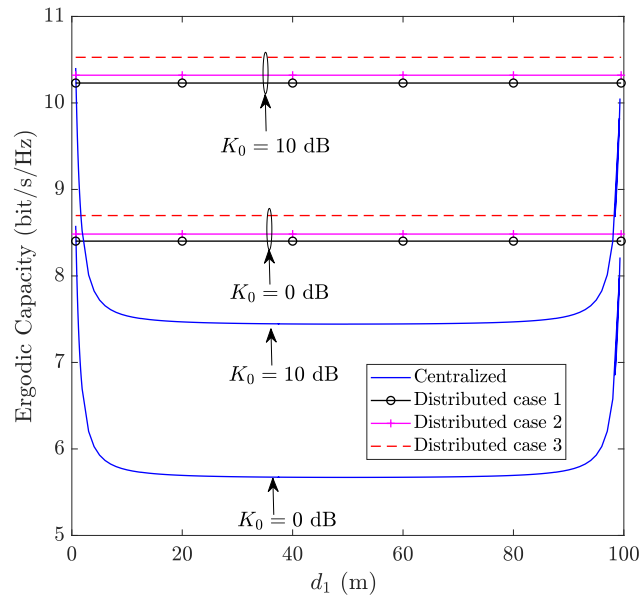
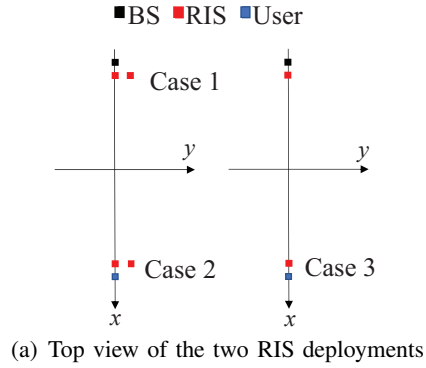
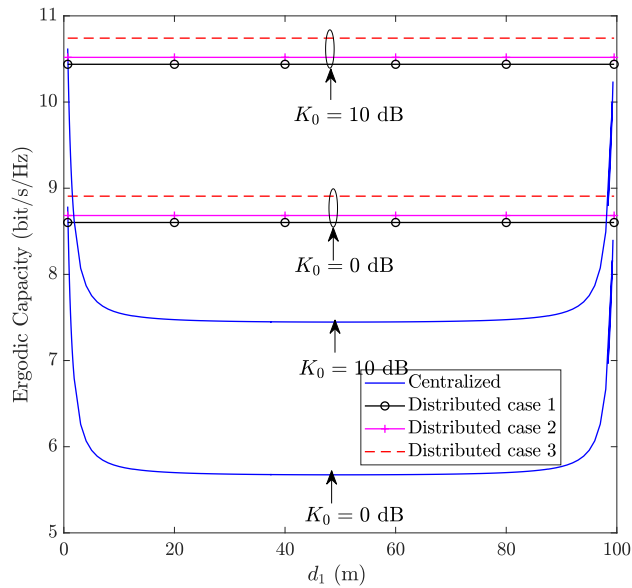
(b) EC of centralized and distributed RIS-aided systems ( $\rho_C = 0.9$ ).(c) EC of centralized and distributed RIS-aided systems ( $\rho_C = 1$ ).

Fig. 8: Comparison of the EC performance for different deployment strategies.

and distributed deployments remain the same regardless of the values  $K_0$ .

## V. CONCLUSION

In this paper, we have studied the ergodic capacity of centralized and distributed RIS-aided communication systems. Considering the effects of near-field/far-field propagation conditions and outdated CSI, we derived accurate closed-form approximations for the ergodic capacity. Moreover, tight lower and upper bounds for the ergodic capacity were derived. Our analysis reveals that the system performance improves with the transmit power, the Rician- $K$  factor, the outdated CSI coefficient and the size of the reflecting elements. Furthermore, the numerical results show that a distributed RIS-aided system usually outperforms a centralized RIS-aided system, and that they provide almost the same ergodic capacity if a single RIS is deployed near the transmitter or near the receiver.

### APPENDIX A

#### PROOF OF COROLLARY 1

Denote  $U_m \triangleq \sqrt{\beta_m^{-1}} |\hat{g}_{Cm}| |h_{Cm}|$ ,  $T \triangleq \rho_C \sum_{m=1}^M U_m$ ,  $Z \triangleq T + \rho_0 |\hat{g}_0|$ ,  $R \triangleq Z^2$ , we have

$$\mathbb{E}(U_m) = \sqrt{\beta_m^{-1}} \Omega_1 \Omega_2,$$

$$\mathbb{E}(U_m^2) = \beta_m^{-1}.$$

Similarly, we can obtain the moments of  $T$ ,  $Z$  as

$$\mathbb{E}(T) = \mathbb{E}\left(\rho_C \sum_{m=1}^M U_m\right) = \rho_C \sum_{m=1}^M \sqrt{\beta_m^{-1}} \Omega_1 \Omega_2,$$

$$\begin{aligned} \mathbb{E}(T^2) &= \mathbb{E}\left(\left(\rho_C \sum_{m=1}^M U_m\right)^2\right) \\ &= \mathbb{E}\left(\rho_C^2 \sum_{m=1}^M U_m^2 + \rho_C^2 \sum_{m=1}^M \sum_{k=1, k \neq m}^M U_m U_k\right) \\ &= \rho_C^2 \sum_{m=1}^M \beta_m^{-1} + \rho_C^2 \sum_{m=1}^M \sum_{k=1, k \neq m}^M \sqrt{\beta_m^{-1} \beta_k^{-1}} (\Omega_1 \Omega_2)^2, \end{aligned}$$



$$\begin{aligned}
\mathbb{E}(Z) &= \mathbb{E}(T + \rho_0 |\hat{g}_0|) = \rho_C \sum_{m=1}^M \sqrt{\beta_m^{-1}} \Omega_1 \Omega_2 + \sqrt{\beta_0^{-1}} \rho_0 \Omega_0, \\
\mathbb{E}(Z^2) &= \mathbb{E}((T + \rho_0 |\hat{g}_0|)^2) = (T^2 + \rho_0^2 |\hat{g}_0|^2 + 2T\rho_0 |\hat{g}_0|) \\
&= \rho_C^2 \sum_{m=1}^M \beta_m^{-1} + \rho_C^2 \sum_{m=1}^M \sum_{k=1, k \neq m}^M \sqrt{\beta_m^{-1} \beta_k^{-1}} (\Omega_1 \Omega_2)^2 + \beta_0^{-1} \rho_0^2 \\
&\quad + 2\sqrt{\beta_0^{-1}} \rho_C \rho_0 \sum_{m=1}^M \sqrt{\beta_m^{-1}} \Omega_0 \Omega_1 \Omega_2. \tag{A.1}
\end{aligned}$$

Then, with the aid of [56, Sec. 2.2.2], the PDF of  $Z$  can be approximated with a Gamma distribution. Therefore, (23) is obtained and the proof is completed.

## APPENDIX B

### PROOF OF COROLLARY 2

We first consider the derivation of  $\sigma_{\text{Ceff}}^2$ . Using (6), we obtain

$$\begin{aligned}
\sigma_{\text{Ceff}}^2 &\triangleq \mathbb{E}(|n_{\text{Ceff}}|^2) = P\bar{\rho}_C^2 \mathbb{E}(|\omega_C \mathbf{B} \Phi_C \mathbf{h}_C|^2) \\
&\quad + P\bar{\rho}_0^2 \beta_0^{-1} \mathbb{E}(|\omega_0|^2) + \mathbb{E}(|n_0|^2). \tag{B.1}
\end{aligned}$$

In particular, we have

$$\mathbb{E}(|n_0|^2) = \sigma_0^2, \tag{B.2}$$

$$\mathbb{E}(|\omega_0|^2) = \sigma_{h_0}^2 = 1 - \Omega_0^2, \tag{B.3}$$

Furthermore, we have

$$\begin{aligned}
\mathbb{E} (|\boldsymbol{\omega}_C \mathbf{B} \boldsymbol{\Phi}_C \mathbf{h}_C|^2) &= \mathbb{E} \left( \left| \sum_{m=1}^M \frac{\omega_{Cm} h_{Cm} e^{j\varphi_{Cm}}}{\sqrt{\beta_m}} \right|^2 \right) \\
&= \mathbb{E} \left( \left| \sum_{m=1}^M \sum_{k=1}^M \frac{\omega_{Cm} h_{Cm} e^{j\varphi_{Cm}}}{\sqrt{\beta_m}} \frac{\omega_{Ck}^* h_{Ck}^* e^{-j\varphi_{Ck}}}{\sqrt{\beta_k}} \right|^2 \right) \\
&= \underbrace{\sum_{m=1}^M \frac{\mathbb{E}(|\omega_{Cm}|^2) \mathbb{E}(|h_{Cm}|^2)}{\beta_m}}_{I_1} \\
&\quad + \underbrace{\sum_{m=1}^M \sum_{k=1, k \neq m}^M \mathbb{E} \left( \frac{\omega_{Cm} h_{Cm} \omega_{Ck}^* h_{Ck}^*}{\sqrt{\beta_m \beta_k}} \right) e^{j(\varphi_{Cm} - \varphi_{Ck})}}_{I_2}. \tag{B.4}
\end{aligned}$$

Since  $\omega_C$ , and  $\mathbf{h}_C$  are independent of each other and  $\mathbb{E}(\omega_{Cm}) = 0$ , we obtain  $I_2 = 0$  and

$$I_1 = \sum_{m=1}^M \sigma_{\tilde{g}_{Cm}}^2 (\sigma_{h_{Cm}}^2 + (\mathbb{E}(|h_{Cm}|^2))) \beta_m^{-1} = (1 - \Omega_2^2) \sum_{m=1}^M \beta_m^{-1}, \tag{B.5}$$

By substituting (B.5) and  $I_2 = 0$  into (B.4), we arrive at

$$\mathbb{E} (|\boldsymbol{\omega}_C \mathbf{B} \boldsymbol{\Phi}_C \mathbf{h}_C|^2) = (1 - \Omega_2^2) \sum_{m=1}^M \beta_m^{-1}. \tag{B.6}$$

By substituting (B.2), (B.3) and (B.6) into (B.1), we prove (28).

Now, we turn our attention to the derivation of the EC in (27). From (22) and employing the integration by parts method, the EC can be rewritten as

$$\bar{C} = \frac{1}{\ln 2} \int_0^\infty \frac{1 - F_\gamma(\gamma)}{1 + \gamma} d\gamma. \tag{B.7}$$

Substituting (26) into (B.7) and using [59, Eq. (07.34.03.0271.01)], [59, Eq. (07.34.03.0613.01)] together with [59, Eq. (07.34.21.0013.01)], the EC can be obtained as in (27).

## APPENDIX C

### PROOF OF COROLLARY 3

By using (8), we obtain

$$\mathbb{E}(\gamma_{C\max}) = \gamma_{C\text{teff}} \mathbb{E}(Z^2). \tag{C.1}$$

Employing (A.1), we obtain the upper bound for the EC in (34). According to (23) and utilizing  $\gamma_{\text{Cmax}} = \gamma_{\text{Cteff}} Z^2$ , we obtain the PDF of  $\gamma_{\text{Cmax}}$  as

$$f_{\gamma_{\text{Cmax}}}(\gamma) = \frac{b_{Z1}^{a_{Z1}}}{2\gamma_{\text{Cteff}}^{a_{Z1}/2} \Gamma(a_{Z1})} (\sqrt{\gamma})^{a_{Z1}-2} e^{-b_{Z1} \sqrt{\frac{\gamma}{\gamma_{\text{Cteff}}}}}. \quad (\text{C.2})$$

With the aid of  $\mathbb{E}(\gamma_{\text{Cmax}}) = \int_0^\infty \gamma f_{\gamma_{\text{Cmax}}}(\gamma) d\gamma$ ,  $\mathbb{E}(\gamma_{\text{Cmax}}^2) = \int_0^\infty \gamma^2 f_{\gamma_{\text{Cmax}}}(\gamma) d\gamma$  and [46, 3.326.3], we derive the mean and variance of  $\gamma_{\text{Cmax}}$  as

$$\begin{aligned} \mathbb{E}(\gamma_{\text{Cmax}}) &= \frac{b_{Z1}^{a_{Z1}}}{2\gamma_{\text{Cteff}}^{a_{Z1}/2} \Gamma(a_{Z1})} \int_0^\infty \gamma (\sqrt{\gamma})^{a_{Z1}-2} e^{-b_{Z1} \sqrt{\frac{\gamma}{\gamma_{\text{Cteff}}}}} d\gamma \\ &= \gamma_{\text{Cteff}} \frac{\Gamma(a_{Z1} + 2)}{b_{Z1}^2 \Gamma(a_{Z1})}, \end{aligned} \quad (\text{C.3})$$

$$\begin{aligned} \mathbb{E}(\gamma_{\text{Cmax}}^2) &= \frac{b_{Z1}^{a_{Z1}}}{2\gamma_{\text{Cteff}}^{a_{Z1}/2} \Gamma(a_{Z1})} \int_0^\infty \gamma^2 (\sqrt{\gamma})^{a_{Z1}-2} e^{-b_{Z1} \sqrt{\frac{\gamma}{\gamma_{\text{Cteff}}}}} d\gamma \\ &= \gamma_{\text{Cteff}}^2 \frac{\Gamma(a_{Z1} + 4)}{b_{Z1}^4 \Gamma(a_{Z1})}, \end{aligned} \quad (\text{C.4})$$

Finally, by utilizing the relation  $\text{Var}(\gamma_{\text{Cmax}}) = \mathbb{E}(\gamma_{\text{Cmax}}^2) - (\mathbb{E}(\gamma_{\text{Cmax}}))^2$ , we obtain the variance in (36).

## APPENDIX D

### PROOF OF COROLLARY 4

By denoting  $X_{lm} \triangleq \sqrt{\beta_{lm}^{-1}} |\hat{g}_{Dlm}| |h_{Dlm}|$ ,  $Y \triangleq \sum_{l=1}^L \sum_{m=1}^{M_l} \rho_{Dl} X_{lm}$  and  $H \triangleq Y + \rho_0 |\hat{g}_0|$ , we have

$$\mathbb{E}(X_{lm}) = \mathbb{E}\left(\sqrt{\beta_{lm}^{-1}} |\hat{g}_{Dlm}| |h_{Dlm}|\right) = \sqrt{\beta_{lm}^{-1}} \Omega_{1l} \Omega_{2l}, \quad (\text{D.1})$$

$$\mathbb{E}(X_{lm}^2) = \beta_{lm}^{-1}, \quad (\text{D.2})$$

$$\begin{aligned} \mathbb{E}(Y) &= \mathbb{E}\left(\sum_{l=1}^L \sum_{m=1}^{M_l} \rho_{Dl} X_{lm}\right) \\ &= \sum_{l=1}^L \sum_{m=1}^{M_l} \rho_{Dl} \mathbb{E}(X_{lm}) = \sum_{l=1}^L \sum_{m=1}^{M_l} \rho_{Dl} \sqrt{\beta_{lm}^{-1}} \Omega_{1l} \Omega_{2l}. \end{aligned} \quad (\text{D.3})$$

$$\begin{aligned}
\mathbb{E}(Y^2) &= \mathbb{E} \left( \left( \sum_{l=1}^L \sum_{m=1}^{M_l} \rho_{Dl} X_{lm} \right)^2 \right) \\
&= \mathbb{E} \left( \sum_{l=1}^L \sum_{m=1}^{M_l} \rho_{Dl}^2 X_{lm}^2 + \sum_{l=1}^L \sum_{m=1}^{M_l} \sum_{k=1, k \neq m}^{M_l} \rho_{Dl}^2 X_{lm} X_{lk} \right. \\
&\quad \left. + \sum_{l=1}^L \sum_{m=1}^{M_l} \left( \rho_{Dl} X_{lm} \sum_{j=1, j \neq l}^L \sum_{k=1}^{M_j} \rho_{Dj} X_{jk} \right) \right) \\
&= \sum_{l=1}^L \sum_{m=1}^{M_l} \frac{\rho_{Dl}^2}{\beta_{lm}} + \sum_{l=1}^L \sum_{m=1}^{M_l} \sum_{k=1, k \neq m}^{M_l} \frac{\rho_{Dl}^2 \Omega_{1l}^2 \Omega_{2l}^2}{\sqrt{\beta_{lm} \beta_{lk}}} \\
&\quad + \sum_{l=1}^L \sum_{m=1}^{M_l} \left( \frac{\rho_{Dl} \Omega_{1l} \Omega_{2l}}{\sqrt{\beta_{lm}}} \sum_{j=1, j \neq l}^L \sum_{k=1}^{M_j} \frac{\rho_{Dj} \Omega_{1j} \Omega_{2j}}{\sqrt{\beta_{lk}}} \right). \tag{D.4}
\end{aligned}$$

$$\mathbb{E}(H) = \mathbb{E}(Y + \rho_0 |\hat{g}_0|) = \sum_{l=1}^L \sum_{m=1}^{M_l} \sqrt{\beta_{lm}^{-1}} \rho_{Dl} \Omega_{1l} \Omega_{2l} + \sqrt{\beta_0^{-1}} \rho_0 \Omega_0. \tag{D.5}$$

$$\begin{aligned}
\mathbb{E}(H^2) &= \mathbb{E}((Y + \rho_0 |\hat{g}_0|)^2) = \mathbb{E}(Y^2 + \beta_0^{-1} \rho_0^2 + 2Y \rho_0 |\hat{g}_0|) \\
&= \sum_{l=1}^L \sum_{m=1}^{M_l} \frac{\rho_{Dl}^2}{\beta_{lm}} + \sum_{l=1}^L \sum_{m=1}^{M_l} \sum_{k=1, k \neq m}^{M_l} \frac{\rho_{Dl}^2 \Omega_{1l}^2 \Omega_{2l}^2}{\sqrt{\beta_{lm} \beta_{lk}}} \\
&\quad + \sum_{l=1}^L \sum_{m=1}^{M_l} \left( \frac{\rho_{Dl} \Omega_{1l} \Omega_{2l}}{\sqrt{\beta_{lm}}} \sum_{j=1, j \neq l}^L \sum_{k=1}^{M_j} \frac{\rho_{Dj} \Omega_{1j} \Omega_{2j}}{\sqrt{\beta_{jk}}} \right) \\
&\quad + \frac{2\rho_0}{\sqrt{\beta_0}} \sum_{l=1}^L \sum_{m=1}^{M_l} \frac{\rho_{Dl} \Omega_{1l} \Omega_{2l}}{\sqrt{\beta_{lm}}} + \frac{\rho_0^2}{\beta_0}. \tag{D.6}
\end{aligned}$$

Then, according to [56, Sec. 2.2.2], the PDF of  $H$  can be tightly approximated by the Gamma distribution which is characterized by two parameters  $a_{H1} \triangleq \frac{(\mathbb{E}(H))^2}{\text{Var}(H)}$ ,  $b_{H1} \triangleq \frac{\mathbb{E}(H)}{\text{Var}(H)}$ . Then, (39) is proved.

APPENDIX E  
PROOF OF COROLLARY 5

The variance of the equivalent noise  $n_{\text{Def}}$  for the distributed deployment can be derived as

$$\begin{aligned} \sigma_{\text{Def}}^2 &\triangleq \mathbb{E} (|n_{\text{Def}}|^2) = P \sum_{l=1}^L \bar{\rho}_{\text{D}l}^2 \mathbb{E} (|\omega_{\text{D}l} \mathbf{B}_{\text{D}l} \Phi_{\text{D}l} \mathbf{h}_{\text{D}l}|^2) \\ &\quad + P \bar{\rho}_0^2 \beta_0^{-1} \mathbb{E} (|\omega_0|^2) + \mathbb{E} (|n_0|^2), \end{aligned} \quad (\text{E.1})$$

where  $\mathbb{E} (|n_0|^2)$  and  $\mathbb{E} (|\omega_0|^2)$  are given in (B.2) and (B.3), respectively. Moreover, we have

$$\begin{aligned} \mathbb{E} (|\omega_{\text{D}l} \mathbf{B}_{\text{D}l} \Phi_{\text{D}l} \mathbf{h}_{\text{D}l}|^2) &= \mathbb{E} \left( \sum_{m=1}^{M_l} \frac{|\omega_{\text{D}lm} \mathbf{h}_{\text{D}lm}|^2}{\sqrt{\beta_{lm}}} \right) \\ &\quad + \mathbb{E} \left( \left| \sum_{m=1}^{M_l} \sum_{k \neq m}^{M_l} \frac{\omega_{\text{D}lm} \mathbf{h}_{\text{D}lm} \omega_{\text{D}lk}^* \mathbf{h}_{\text{D}lk}^* e^{j(\varphi_{lm} - \varphi_{lk})}}{\sqrt{\beta_{lm} \beta_{lk}}} \right|^2 \right) \\ &= \underbrace{\sum_{m=1}^{M_l} \frac{\mathbb{E} (|\omega_{\text{D}lm}|^2) \mathbb{E} (|\mathbf{h}_{\text{D}lm}|^2)}{\beta_{lm}}}_{I_3} \\ &\quad + \underbrace{\sum_{m=1}^{M-1} \sum_{k=1, k \neq m}^M \mathbb{E} \left( \frac{\omega_{\text{D}lm} \mathbf{h}_{\text{D}lm} \omega_{\text{D}lk}^* \mathbf{h}_{\text{D}lk}^*}{\sqrt{\beta_{lm} \beta_{lk}}} \right) e^{j(\varphi_{lm} - \varphi_{lk})}}_{I_4}. \end{aligned} \quad (\text{E.2})$$

Due to the fact that  $\omega_{\text{D}l}$ , and  $\mathbf{h}_{\text{D}l}$  are independent of each other, we obtain  $I_4=0$  and

$$I_3 = \sum_{m=1}^{M_l} \beta_{lm}^{-1} \sigma_{\text{gD}lm}^2 (\sigma_{\text{hD}lm}^2 + \mathbb{E}^2 (|\mathbf{h}_{\text{D}lm}|)) = (1 - \Omega_{2l}^2) \sum_{m=1}^{M_l} \beta_{lm}^{-1}. \quad (\text{E.3})$$

Substituting (E.2), (E.3),  $I_4=0$ , (B.2) and (B.3) into (E.1), we arrive at (44).

Next, by exploiting a similar methodology as for the derivation of (26), we arrive at

$$F_{\gamma_{\text{Dmax}}} (\gamma) = 1 - \frac{1}{\Gamma (a_{H1})} \Gamma \left( a_{H1}, b_{H1} \sqrt{\frac{\gamma}{\gamma_{\text{Dteff}}}} \right). \quad (\text{E.4})$$

Substituting (E.4) into (B.7) and with the aid of [59, Eq. (07.34.03.0271.01)], [59, Eq. (07.34.03.0613.01)] and [59, Eq. (07.34.21.0013.01)], we obtain (43).

APPENDIX F  
PROOF OF COROLLARY 6

We can rewrite (18) as

$$\mathbb{E}(\gamma_{D_{\max}}) = \gamma_{D_{\text{teff}}} \mathbb{E}(H^2). \quad (\text{F.1})$$

Next, by employing (41), we obtain (47). Then,  $\text{Var}(\gamma_{D_{\max}})$  is obtained by using the same approach as for the derivation of (36).

REFERENCES

- [1] J. Zhang, E. Björnson, M. Matthaiou, D. W. K. Ng, H. Yang, and D. J. Love, “Prospective multiple antenna technologies for beyond 5G,” *IEEE J. Sel. Areas Commun.*, vol. 38, no. 8, pp. 1637–1660, Aug. 2020.
- [2] Q. Wu and R. Zhang, “Beamforming optimization for wireless network aided by intelligent reflecting surface with discrete phase shifts,” *IEEE Trans. Commun.*, vol. 68, no. 3, pp. 1838–1851, Mar. 2020.
- [3] M. Di Renzo *et al.*, “Smart radio environments empowered by reconfigurable intelligent surfaces: How it works, state of research, and the road ahead,” *IEEE J. Sel. Areas Commun.*, vol. 38, no. 11, pp. 2450–2525, Nov. 2020.
- [4] E. Basar, M. Di Renzo, J. De Rosny, M. Debbah, M. Alouini, and R. Zhang, “Wireless communications through reconfigurable intelligent surfaces,” *IEEE Access*, vol. 7, pp. 116 753–116 773, Aug. 2019.
- [5] C. Huang *et al.*, “Holographic MIMO surfaces for 6G wireless networks: Opportunities, challenges, and trends,” *IEEE Wireless Commun.*, vol. 27, no. 5, pp. 118–125, Oct. 2020.
- [6] Y. Liu, X. Liu, X. Mu, T. Hou, J. Xu, M. Di Renzo, and N. Al-Dhahir, “Reconfigurable intelligent surfaces: Principles and opportunities,” *IEEE Commun. Surveys. Tuts.*, vol. 22, no. 3, pp. 1546–1577, May 2021.
- [7] Y. Chen, Y. Wang, J. Zhang, and Z. Li, “Resource allocation for intelligent reflecting surface aided vehicular communications,” *IEEE Trans. Veh. Technol.*, vol. 69, no. 10, pp. 12 321–12 326, Oct. 2020.
- [8] L. Yang, F. Meng, J. Zhang, M. O. Hasna, and M. Di Renzo, “On the performance of RIS-assisted dual-hop UAV communication systems,” *IEEE Trans. Veh. Technol.*, vol. 69, no. 9, pp. 10 385–10 390, Sep. 2020.
- [9] M. Di Renzo *et al.*, “Smart radio environments empowered by reconfigurable AI meta-surfaces: An idea whose time has come,” *EURASIP J. Wireless Commun. Netw.*, vol. 2019, no. 129, pp. 1–20, May 2019.
- [10] M. Di Renzo *et al.*, “Reconfigurable intelligent surfaces vs. relaying: Differences, similarities, and performance comparison,” *IEEE Open J. Commun. Soc.*, vol. 1, pp. 798–807, Jun. 2020.
- [11] L. Yang, Y. Yang, M. O. Hasna, and M.-S. Alouini, “Coverage, probability of SNR gain, and DOR analysis of RIS-aided communication systems,” *IEEE Wireless Commun. Lett.*, vol. 9, no. 8, pp. 1268–1272, Aug. 2020.
- [12] T. Van Chien, L. T. Tu, S. Chatzinotas, and B. Ottersten, “Coverage probability and ergodic capacity of intelligent reflecting surface-enhanced communication systems,” *IEEE Commun. Lett.*, vol. 25, no. 1, pp. 69–73, Jan. 2021.
- [13] L. Yang, F. Meng, Q. Wu, D. B. da Costa, and M.-S. Alouini, “Accurate closed-form approximations to channel distributions of RIS-aided wireless systems,” *IEEE Wireless Commun. Lett.*, vol. 9, no. 11, pp. 1985–1989, Nov. 2020.
- [14] A. M. Salhab and M. H. Samuh, “Accurate performance analysis of reconfigurable intelligent surfaces over rician fading channels,” *IEEE Wireless Commun. Lett.*, vol. 10, no. 5, pp. 1051–1055, May 2021.
- [15] D. Kudathanthirige, D. Gunasinghe, and G. Amarasinghe, “Performance analysis of intelligent reflective surfaces for wireless communication,” in *Proc. IEEE ICC*, Jun. 2020, pp. 1–6.

- [16] S. Lin, B. Zheng, G. C. Alexandropoulos, M. Wen, M. Di Renzo, and F. Chen, "Reconfigurable intelligent surfaces with reflection pattern modulation: Beamforming design and performance analysis," *IEEE Trans. Wireless Commun.*, vol. 20, no. 2, pp. 741–754, Feb. 2021.
- [17] T. Wang, G. Chen, J. P. Coon, and M.-A. Badiu, "Chernoff bounds and saddlepoint approximations for the outage probability in intelligent reflecting surface assisted communication systems," [Online]. Available: <https://arxiv.org/abs/2008.05447>.
- [18] T. Wang, G. Chen, J. P. Coon, and M.-A. Badiu, "Study of intelligent reflective surface assisted communications with one-bit phase adjustments," in *IEEE Global Commun. Conf. (GLOBECOM)*, Dec. 2020, pp. 1–6.
- [19] R. C. Ferreira, M. S. P. Facina, F. A. P. De Figueiredo, G. Fraidenraich, and E. R. De Lima, "Bit error probability for large intelligent surfaces under double-Nakagami fading channels," *IEEE Open J. Commun. Soc.*, vol. 1, pp. 750–759, May 2020.
- [20] I. Trigui, E. K. Agbogla, M. Benjillali, W. Ajib, and W.-P. Zhu, "Bit error rate analysis for reconfigurable intelligent surfaces with phase errors," *IEEE Commun. Lett.*, vol. 25, no. 7, pp. 2176–2180, Jul. 2021.
- [21] M.-A. Badiu and J. P. Coon, "Communication through a large reflecting surface with phase errors," *IEEE Wireless Commun. Lett.*, vol. 9, no. 2, pp. 184–188, Feb. 2020.
- [22] D. Li, "Ergodic capacity of intelligent reflecting surface-assisted communication systems with phase errors," *IEEE Commun. Lett.*, vol. 24, no. 8, pp. 1646–1650, Aug. 2020.
- [23] A.-A. A. Boulogeorgos and A. Alexiou, "Ergodic capacity analysis of reconfigurable intelligent surface assisted wireless systems," in *Proc. IEEE 3rd 5G World Forum (5GWF)*, 2020, pp. 395–400.
- [24] P. Xu, G. Chen, Z. Yang, and M. Di Renzo, "Reconfigurable intelligent surfaces-assisted communications with discrete phase shifts: How many quantization levels are required to achieve full diversity?" *IEEE Wireless Commun. Lett.*, vol. 10, no. 2, pp. 358–362, Feb. 2020.
- [25] X. Qian, M. Di Renzo, J. Liu, A. Kammoun, and M.-S. Alouini, "Beamforming through reconfigurable intelligent surfaces in single-user MIMO systems: SNR distribution and scaling laws in the presence of channel fading and phase noise," *IEEE Wireless Commun. Lett.*, vol. 10, no. 1, pp. 77–81, Jan. 2021.
- [26] P. Dharmawansa, S. Atapattu, and M. Di Renzo, "Performance analysis of a two-tile reconfigurable intelligent surface assisted  $2 \times 2$  MIMO system," *IEEE Wireless Commun. Lett.*, vol. 10, no. 3, pp. 493–497, Mar. 2021.
- [27] I. Trigui, W. Ajib, and W. Zhu, "A comprehensive study of reconfigurable intelligent surfaces in generalized fading," [Online]. Available: <https://arxiv.org/abs/2004.02922>.
- [28] I. Trigui, W. Ajib, W.-P. Zhu, and M. Di Renzo, "Performance evaluation and diversity analysis of RIS-assisted communications over generalized fading channels in the presence of phase noise," [Online]. Available: <https://arxiv.org/abs/2011.12260>.
- [29] M. Jung, W. Saad, Y. Jang, G. Kong, and S. Choi, "Performance analysis of large intelligent surfaces (LISs): Asymptotic data rate and channel hardening effects," *IEEE Trans. Wireless Commun.*, vol. 19, no. 3, pp. 2052–2065, Mar. 2020.
- [30] L. Yang, J. Yang, W. Xie, M. O. Hasna, T. Tsiftsis, and M. Di Renzo, "Secrecy performance analysis of RIS-aided wireless communication systems," *IEEE Trans. Veh. Technol.*, vol. 69, no. 10, pp. 12 296–12 300, Oct. 2020.
- [31] H. Du, J. Zhang, J. Cheng, and B. Ai, "Millimeter wave communications with reconfigurable intelligent surfaces: Performance analysis and optimization," *IEEE Trans. Commun.*, vol. 69, no. 4, pp. 2752–2768, Apr. 2021.
- [32] S. Atapattu, R. Fan, P. Dharmawansa, G. Wang, J. Evans, and T. A. Tsiftsis, "Reconfigurable intelligent surface assisted two-way communications: Performance analysis and optimization," *IEEE Trans. Commun.*, vol. 68, no. 10, pp. 6552–6567, Oct. 2020.
- [33] Q. Tao, J. Wang, and C. Zhong, "Performance analysis of intelligent reflecting surface aided communication systems," *IEEE Commun. Lett.*, vol. 24, no. 11, pp. 2464–2468, 2020.

- [34] F. H. Danufane, M. Di Renzo, J. De Rosny, and S. Tretyakov, "On the path-loss of reconfigurable intelligent surfaces: An approach based on green's theorem applied to vector fields," *IEEE Trans. Commun.*, vol. 69, no. 8, pp. 5573–5592, Aug. 2021.
- [35] J. Zhang, H. Du, Q. Sun, B. Ai, and D. W. K. Ng, "Physical layer security enhancement with reconfigurable intelligent surface-aided networks," *IEEE Trans. Inf. Forensic Secur.*, vol. 16, pp. 3480–3495, 2021.
- [36] L. Yang, Y. Yang, D. B. da Costa, and I. Trigui, "Outage probability and capacity scaling law of multiple RIS-aided networks," *IEEE Wireless Commun. Lett.*, vol. 10, no. 2, pp. 256–260, Feb. 2021.
- [37] I. Yildirim, A. Uyrus, and E. Basar, "Modeling and analysis of reconfigurable intelligent surfaces for indoor and outdoor applications in future wireless networks," *IEEE Trans. Commun.*, vol. 69, no. 2, pp. 1290–1301, Feb. 2020.
- [38] T. N. Do, G. Kaddoum, T. L. Nguyen, D. B. da Costa, and Z. J. Haas, "Multi-RIS-aided wireless systems: Statistical characterization and performance analysis," *IEEE Trans. Commun.*, vol. 69, no. 12, pp. 8641–8658, Dec. 2021.
- [39] D. L. Galappathige, D. Kudathanthirige, and G. A. A. Baduge, "Performance analysis of distributed intelligent reflective surfaces for wireless communications," [Online]. Available: <https://arxiv.org/abs/2010.12543>.
- [40] S. Zhang and R. Zhang, "Intelligent reflecting surface aided multi-user communication: Capacity region and deployment strategy," *IEEE Trans. Commun.*, vol. 69, no. 9, pp. 5790–5806, Sept. 2021.
- [41] A. Abrardo, D. Dardari, and M. Di Renzo, "Intelligent reflecting surfaces: Sum-rate optimization based on statistical position information," *IEEE Trans. Commun.*, vol. 69, no. 10, pp. 7121–7136, Oct. 2021.
- [42] X. Yu, D. Xu, Y. Sun, D. W. K. Ng, and R. Schober, "Robust and secure wireless communications via intelligent reflecting surfaces," *IEEE J. Sel. Areas Commun.*, vol. 38, no. 11, pp. 2637–2652, Nov. 2020.
- [43] H. Yang, Z. Xiong, J. Zhao, D. Niyato, L. Xiao, and Q. Wu, "Deep reinforcement learning-based intelligent reflecting surface for secure wireless communications," *IEEE Trans. Wireless Commun.*, vol. 20, no. 1, pp. 375–388, Jan. 2021.
- [44] R. Hashemi, S. Ali, N. H. Mahmood, and M. Latva-aho, "Deep reinforcement learning for practical phase shift optimization in RIS-aided MISO URLLC systems," [Online]. Available: <https://arxiv.org/abs/2110.08513>.
- [45] A. Zappone, M. Di Renzo, F. Shams, X. Qian, and M. Debbah, "Overhead-aware design of reconfigurable intelligent surfaces in smart radio environments," *IEEE Trans. Wireless Commun.*, vol. 20, no. 1, pp. 126–141, Jan. 2021.
- [46] I. S. Gradshteyn and I. M. Ryzhik, *Table of Integrals, Series and Products*, 7th ed. Burlington, MA, USA: Academic, 2007.
- [47] S. A. Tegos, D. Tyrovolas, P. D. Diamantoulakis, and G. K. Karagiannidis, "On the distribution of the sum of double-Nakagami- $m$  random vectors and application in randomly reconfigurable surfaces," [Online]. Available: <https://arxiv.org/abs/2102.05591>.
- [48] N. Yang, M. Elkashlan, P. L. Yeoh, and J. Yuan, "Multiuser MIMO relay networks in Nakagami- $m$  fading channels," *IEEE Trans. commun.*, vol. 60, no. 11, pp. 3298–3310, Nov. 2012.
- [49] P. Kumar and P. Sahu, "Analysis of  $M$ -PSK with MRC receiver over  $\kappa - \mu$  fading channels with outdated CSI," *IEEE Wireless Commun. Lett.*, vol. 3, no. 6, pp. 557–560, Dec. 2014.
- [50] Q.-U.-A. Nadeem, H. Alwazani, A. Kammoun, A. Chaaban, M. Debbah, and M.-S. Alouini, "Intelligent reflecting surface-assisted multi-user MISO communication: Channel estimation and beamforming design," *IEEE Open J. Commun. Soc.*, vol. 1, pp. 661–680, May 2020.
- [51] N. K. Kundu and M. R. McKay, "Channel estimation for reconfigurable intelligent surface aided MISO communications: From LMMSE to deep learning solutions," *IEEE Open J. Commun. Soc.*, vol. 2, pp. 471–487, Mar. 2021.
- [52] G. Gradoni and M. Di Renzo, "End-to-end mutual coupling aware communication model for reconfigurable intelligent surfaces: An electromagnetic-compliant approach based on mutual impedances," *IEEE Wireless Commun. Lett.*, vol. 10, no. 5, pp. 938–942, May 2021.



- [53] W. Tang, X. Chen, M. Z. Chen, J. Y. Dai, Y. Han, M. Di Renzo, S. Jin, Q. Cheng, and T. J. Cui, "Path loss modeling and measurements for reconfigurable intelligent surfaces in the millimeter-wave frequency band," [Online]. Available: <https://arxiv.org/abs/2101.08607>.
- [54] A. Abrardo, D. Dardari, M. Di Renzo, and X. Qian, "MIMO interference channels assisted by reconfigurable intelligent surfaces: Mutual coupling aware sum-rate optimization based on a mutual impedance channel model," *IEEE Wireless Commun. Lett.*, vol. 10, no. 12, pp. 2624–2628, Dec. 2021.
- [55] V. Arun and H. Balakrishnan, "Rfocus: Beamforming using thousands of passive antennas," in *USENIX Symposium on Networked Systems Design and Implementation*, Feb. 2020, pp. 1047–1061.
- [56] S. Primak, V. Kontorovich, and V. Lyandres, *Stochastic methods and their applications to communications: stochastic differential equations approach*. West Sussex, U.K.: Wiley, 2004.
- [57] M. Abramowitz and I. A. Stegun, *Handbook of mathematical functions with formulas, graphs, and mathematical tables*, 9th ed. New York: Dover, 1972.
- [58] J. G. Proakis and M. Salehi, *Digital Communications*, 4th ed. New York, NY, USA: McGraw Hill, 2001.
- [59] Wolfram, "The Wolfram functions site," [Online]. Available: <http://functions.wolfram.com>.